AD-A075 362 NAVAL RESEARCH LAB WASHINGTON DC F/G 18/1
THEORY OF ELECTRON CYCLOTRON RESONANCE HEATING OF TOKAMAK PLASM--ETC(U)
SEP 79 E OTT, B HUI, K R CHU
UNCLASSIFIED NRL-MR-4028 NL

1 OF 1
ADA 075362

END
DATE FILMED
11-79
DDC

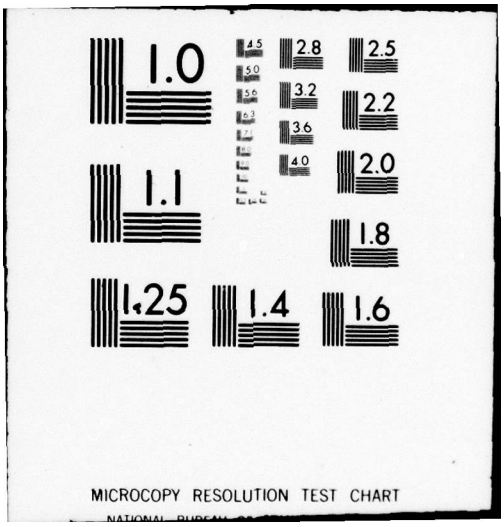
1.0
1.1
1.25
1.4
1.6
1.8
2.0
2.2
2.5
2.8
3.2
3.6
4.0
4.5
5.0
5.6
6.3
MICROCOPY RESOLUTION TEST CHART

LEVEL II

NRL Memorandum Report 4028

Theory of Electron Cyclotron Resonance Heating of Tokamak Plasmas

EDWARD OTT, BERTRAM HUI AND K. R. CHU

Plasma Physics Division

(Interim rept.)

19 Sept 1979

70

NAVAL RESEARCH LABORATORY
Washington, D.C.

251 950

SECURITY CLASSIFICATION OF THIS PAGE (When Data Entered)

REPORT DOCUMENTATION PAGE		READ INSTRUCTIONS BEFORE COMPLETING FORM
1. REPORT NUMBER NRL Memorandum Report 4028	2. GOVT ACCESSION NO.	3. RECIPIENT'S CATALOG NUMBER
4. TITLE (and Subtitle) THEORY OF ELECTRON CYCLOTRON RESONANCE HEATING OF TOKAMAK PLASMAS		5. TYPE OF REPORT & PERIOD COVERED Interim report on a continuing NRL Problem 6. PERFORMING ORG. REPORT NUMBER
7. AUTHOR(s) Edward Ott*, Bertram Hui and K. R. Chu		8. CONTRACT OR GRANT NUMBER(s)
9. PERFORMING ORGANIZATION NAME AND ADDRESS Naval Research Laboratory Washington, D.C. 20375		10. PROGRAM ELEMENT, PROJECT, TASK AREA & WORK UNIT NUMBERS NRL Problem 67H02-37
11. CONTROLLING OFFICE NAME AND ADDRESS U.S. Department of Energy Washington, D.C. 20545		12. REPORT DATE September 19, 1979 13. NUMBER OF PAGES 69
14. MONITORING AGENCY NAME & ADDRESS(if different from Controlling Office)		15. SECURITY CLASS. (of this report) UNCLASSIFIED 15a. DECLASSIFICATION/DOWNGRADING SCHEDULE

16. DISTRIBUTION STATEMENT (of this Report)

Approved for public release; distribution unlimited.

17. DISTRIBUTION STATEMENT (of the abstract entered in Block 20, if different from Report)

18. SUPPLEMENTARY NOTES

*Also at University of Maryland, College Park, Maryland 20742

19. KEY WORDS (Continue on reverse side if necessary and identify by block number)

tokamaks
plasma heating
electron cyclotron resonance
parametric instabilities

20. ABSTRACT (Continue on reverse side if necessary and identify by block number)

A theoretical study of tokamak plasma heating by the electron cyclotron resonance is presented. The density limitations imposed by accessibility are first reviewed. Then the predictions of linear theory (including relativistic effects on the wave absorption) are examined via solutions of the ray equations in a toroidal tokamak equilibrium. These solutions indicate quite favorable characteristics for large tokamaks. Finally, the possibilities of scattering of the incident heating wave by existing drift-wave-type fluctuations and of parametric instability are examined; it is tentatively concluded that parametric instabilities and wave scattering should not be important in typical situations of interest.

DD FORM 1 JAN 73 1473 EDITION OF 1 NOV 65 IS OBSOLETE
S/N 0102-014-6601

SECURITY CLASSIFICATION OF THIS PAGE (When Data Entered)

CONTENTS

THEORY OF ELECTRON CYCLOTRON RESONANCE HEATING OF TOKAMAK PLASMAS

I. INTRODUCTION

Radio frequency plasma heating is of great potential importance in controlled fusion research. Heating at the electron cyclotron frequency is one form of plasma heating which offers many potential advantages. Until recently, however, electron cyclotron resonance heating has received relatively little attention, primarily because efficient powerful microwave sources in the millimeter wavelength range have not been available. This situation is now changing due to the development of the "gyrotron" device both in this country and in the Soviet Union [1]. The gyrotron produces microwave power by the interaction of a high energy anisotropic electron beam with electromagnetic waves via the cyclotron resonance. In contrast with conventional tubes, no cavity resonance is involved, and thus much shorter wavelengths can, in principle, be obtained. Initial tokamak plasma heating experiments at the electron cyclotron frequency have now been carried out, and more are planned.[2]

Motivated by these developments we (and others[3]) have attempted a theoretical study of *tokamak* plasma heating by externally launched electromagnetic waves whose frequency matches the electon cyclotron frequency in the interior of the device. Section II reviews the basic limitations imposed by wave accessibility to the center of the tokamak. It is shown that a density limit for accessibility exists. In Sec. III we utilize the ray equations to obtain the wave propagation and energy deposition in a self-consistent tokamak equilibrium (this represents the first such study utilizing a real toroidal plasma equilibrium and including important relativistic

Manuscript submitted June 21, 1979.

effects on the wave absorption). We find several favorable features of this heating method. Sections IV and V investigate two possible mechanisms which might substantially alter the favorable picture obtained in Sec. III: scattering of the incident heating wave by low frequency density fluctuations existing in the tokamak (e.g. drift waves), and the excitation of parametric instabilities by the heating wave. Our investigation suggests that these two mechanisms should *not*, in fact, pose a serious problem for electron cyclotron heating of tokamak plasmas. In particular, the threshold incident power density for the excitation of parametric instabilities should far exceed the actual incident power density to be expected in typical situations. Section VI summarizes results and presents conclusions.

II. REVIEW OF ACCESSIBILITY

For simplicity, in this section we consider a straight plasma cylinder with density $N(r)(dN/dr<0$ and $N(a)\equiv 0)$, and magnetic field $\mathbf{B} = B(r,\theta)\,\mathbf{z}_o$. To simulate the toroidal vacuum field dependence on the major radius we take $B=B_o(1-x/R_o)^{-1}$ where $x=-r\cos\theta$ and R_o is the major radius of the torus. Furthermore, we assume incident waves launched at $\theta=0$ or $\theta=\pi$ with no θ component of the incident wavenumber ($k_\theta=0$). Since $\mathbf{B}$ has no θ component, k_θ remains zero as the wave propagates inward. (Note that these simplifications are not made in our ray tracing calculations to be presented in Sec. III.)

A. Normal Incidence

a. Ordinary mode: The dispersion relation is

$$\eta^2 = 1-X$$

where $\eta^2 = k^2c^2/\omega^2$, $X = \omega_p^2/\omega^2$, ω_p is the plasma frequency, $\mathbf{k}$ is the wavevector, c is the speed of light and ω is the wave frequency. To avoid reflection we require $X_o < 1$ (Fig. 1), where X_o is X at $r=0$. For $\omega=\omega_{ce}^0$ the condition is $\omega_{po} < \omega_{ce}^0$, where ω_{po} and ω_{ce}^0 are the plasma

frequency and the electron cyclotron frequency (ω_{ce}) evaluated at $r=0$. [For first harmonic heating, $\omega=2\omega_{ce}^0$, the condition becomes $\omega_{po} < 2\omega_{ce}^0$ and heating of higher density plasmas becomes possible. First harmonic heating will, however, not be considered in this paper.]

b. Extraordinary mode: The dispersion relation is

$$\eta^2 = 1-[X(1-X)/(1-X-Y^2)]$$

where $Y = \omega_{ce}/\omega$. The zeros of η^2 (turning points) are located at $X = 1 \pm Y$. A pole of η^2 (resonance) is located at $X = 1-Y^2$ and is the condition for upper hybrid resonance. For $\omega = \omega_{ce}^0$, $Y \cong (1-x/R_0)^{-1}$ and η^2 as a function of x is plotted in Fig. 2(a) for $X_0 \lesssim 2$. We see that an extraordinary wave launched from the low magnetic field side ($x=-a$) always encounters a turning point (followed by the upper hybrid resonance) near the plasma edge. Thus the extraordinary mode should be launched from the high magnetic field side where it will pass through the cyclotron resonant absorption region near $x=0$. If $X_0>2$, the wave will be reflected for both low and high field side injections (Fig. 2(b)).

B. Oblique Incidence

The dispersion relation is given by [4]

$$q^2 = 1-S^2-X\left\{1-\frac{Y^2(1-S^2)}{2(1-X)} \pm \frac{Y^2(1-S^2)}{2(1-X)}\left[1+\frac{4S^2(1-X)}{Y^2(1-S^2)^2}\right]^{1/2}\right\}^{-1}, \qquad (1)$$

where $q \equiv ck_\perp/\omega$, $S=\sin\Theta=k_\parallel c/\omega$, Θ is the angle of incidence (we have looked at normal incidence $S=0$ in Sec. A), and $k_\perp$ and $k_\parallel$ denote components of k perpendicular and parallel to **B**. The plus sign in front of the square root is used for the ordinary mode, and the minus sign for the extraordinary mode (this can be seen by letting $S^2 \to 0$ in (1).)

To find the reflection points, we set $q^2 = 0$ in (1) and get

$$\mp \frac{Y^2(1-S^2)}{2(1-X)} \left[1+ \frac{4(1-X)S^2}{Y^2(1-S^2)^2}\right]^{1/2}_3 = 1- \frac{Y^2(1-S^2)}{2(1-X)} - \frac{X}{1-S^2}, \tag{2}$$

where the minus sign corresponds to the ordinary wave and the plus sign to the extraordinary wave. Squaring both sides and simplifying, we get three reflection points,

$$X_1 = 1, \tag{3}$$

$$X_2 = (1-S^2)(1+Y), \tag{4}$$

$$X_3 = (1-S^2)(1-Y). \tag{5}$$

Now the task is to identify which of these roots corresponds to the ordinary mode (minus sign in (2)) and which to the extraordinary mode (plus sign in (2)). This can be done by substituting (3)-(5) back into (2). We find that X_1 always corresponds to the ordinary wave, X_3 always corresponds to the extraordinary wave, and X_2 corresponds either to the ordinary or the extraordinary wave depending on the angle of incidence. X_2 is an ordinary wave reflection if $S^2 > Y/(Y+2)$, and it is an extraordinary wave reflection if $S^2 < Y/(Y+2)$.

Resonance ($q^2 \to \infty$) occurs when the denominator of (1) is zero. As for $S^2 = 0$ this happens only for the extraordinary wave at the upper hybrid resonance

$$X = X_r \equiv 1 - Y^2 . \tag{6}$$

Mode conversion (i.e. transfering from the extraordinary root to the ordinary root) can occur when the square root in (1) becomes zero. This occurs at

$$X = X_c \equiv 1 + Y^2 \frac{(1-S^2)^2}{4S^2}. \tag{7}$$

One example of mode conversion is if one propagates an extraordinary mode from high field side with $Y_0 = 1$,

$$\left(\frac{\omega_{po}}{\omega_{ce}^{0}}\right)^2 \gtrsim 1 + \frac{1-S^2}{4S^2},$$

and $X_2 < 1$, then the wave will be mode converted to ordinary wave before reaching the upper hybrid resonance. The ordinary wave is reflected at $X=X_1$, moves back to the mode conversion point, and is converted back to extraordinary wave which then propagates back towards the high field side (Fig. 3).

In electron cyclotron resonance heating experiments, we want to avoid all reflection, resonance, and mode conversion points before reaching the center of the torus where maximum absorption occurs. By examination of the expressions for X_1, X_2, X_3, X_r and X_c we find that this can be achieved for $Y_0=1$ if

$$X_0 \lesssim \begin{cases} 2\,(1-S^2), & \text{for } S^2 \lesssim 1/3, \\ 1+\dfrac{(1-S^2)^2}{4S^2}, & \text{for } S^2 \gtrsim 1/3, \end{cases} \tag{8}$$

for the extraordinary wave mode launched from the high magnetic field side, and if

$$X_0 \lesssim \begin{cases} 1, & \text{for } S^2 \lesssim 1/2, \\ 2(1-S^2), & \text{for } S^2 \gtrsim 1/2, \end{cases} \tag{9}$$

for the ordinary wave mode (launched from either side). These accessibility conditions are displayed graphically in Fig. 4. [Note that the extraordinary wave with $Y_0 = 1$ is never accessible when launched from the low magnetic field side since it will always encounter the reflection $X=X_3$ close to the plasma edge and the resonance $X=X_r$ soon after (as in Fig. 2).]

In order to discuss the accessibility problem for a reactor plasma it is instructive to express ω_p^2/ω_{ce}^2 in terms of β, the ratio of plasma to magnetic field pressure,

$$\omega_p^2/\omega_{ce}^2 = 1.25\ (\beta/10\%)\ (10\ \text{keV}/T_e),$$

where we have assumed equal electron and ion temperatures, $T_e = T_i$. It is currently thought that an upper limit on β is set by the stability of the plasma to magnetohydrodynamic ballooning modes. For example, if the central β is limited to below 16% at $T_e = 10$ keV, then the extraordinary mode is necessarily accessible, while for an 8% limit both the ordinary and the extraordinary modes are accessible.

III. LINEAR THEORY OF WAVE PROPAGATION AND ENERGY DEPOSITION

In this section we utilize the geometrical optics approximation to study the propagation and energy deposition of ordinary and extraordinary mode waves in a tokamak plasma. Our formulation will be valid if the plasma inhomogenity scale length and the damping length of the wave greatly exceed the wavelength of the wave. These conditions are well-satisfied in all the cases studied. In Sec. III (a) we discuss the formulation of the ray equations in toroidal coordinates, the local dispersion and damping of the waves, and the self-consistent tokamak equilibrium used. Section III (b) presents and discusses the results of computer calculations based on the equations developed in Sec. III (a) and Appendix A.

A. Formulation

We consider waves satisfying a local dispersion relation $D(\omega - i\gamma, \mathbf{r}, \mathbf{k}) = 0$, where ω and γ are the real frequency and damping rate of the wave and $\mathbf{k}$ is the wavenumber. D can be separated into two parts $D = D_r + i D_i$ where D_r and D_i are real for $\gamma = 0$. Then for $\gamma \ll \omega$ we can approximate ω as the solution of $D_r(\omega, \mathbf{r}, \mathbf{k}) = 0$ and γ as $\gamma \equiv \Gamma(\mathbf{r}, \mathbf{k}) = D_i(\omega, \mathbf{r}, \mathbf{k})\,(\partial D_r/\partial\omega)^{-1}$. In the geometrical optics limit the orbit trajectory and damping of the energy in a wave packet are then given by the ray equations.[5]

$$\frac{d\mathbf{k}}{d\tau} = -\frac{\partial D_r}{\partial \mathbf{r}}, \quad \frac{d\mathbf{r}}{d\tau} = \frac{\partial D_r}{\partial \mathbf{k}}, \tag{10a,b}$$

$$\frac{dt}{d\tau} = -\frac{\partial D_r}{\partial \omega}, \quad \frac{dw}{dt} = -2\Gamma w, \tag{10c,d}$$

where w is the energy in the wave packet. The quantity τ is a measure of the distance along the ray trajectory. Equations (10b) and (10c) yield the usual group velocity: $d\mathbf{r}/dt = -(\partial D_r/\partial \mathbf{k})/(\partial D_r/\partial \omega) = \partial\omega/\partial\mathbf{k}$. Note that in Cartesian coordinates Eqs. (10a,b) are identical to Hamilton's equations of motion for a particle with momentum $\mathbf{k}$ and Hamiltonian D_r, $dk_j/d\tau = -\partial D_r/\partial x_j$ and $dx_j/d\tau = \partial D_r/\partial k_j$. We now introduce the usual toroidal coordinates (r, θ, ϕ), where r is the minor radial position, θ is the poloidal angle, and ϕ is the toroidal angle. The distance from the major axis of the torus to a point (r, θ, ϕ) is $R = R_0 + r\cos\theta$. It is convenient to preserve the Hamiltonian form of (10a, b) which exists in Cartesian geometry by utilizing momenta variables which are cannonically conjugate to (r, θ, ϕ). Therefore we introduce k_r, $m = r\,k_\theta$ and $n = R\,k_\phi$ where (k_r, k_θ, k_ϕ) are the (r, θ, ϕ) components of $\mathbf{k}$. In terms of (r, θ, ϕ) and their connonically conjugate "momenta" (k_r, m, n) the ray equations (10a,b) become[6,7]

$$\frac{dr}{d\tau} = \frac{\partial D_r}{\partial k_r}, \quad \frac{d\theta}{d\tau} = \frac{\partial D_r}{\partial m}, \quad \frac{d\phi}{d\tau} = \frac{\partial D_r}{\partial n},$$
$$\frac{dk_r}{d\tau} = -\frac{\partial D_r}{\partial r}, \quad \frac{dm}{d\tau} = -\frac{\partial D_r}{\partial \theta}, \quad \frac{dn}{d\tau} = 0, \tag{11}$$

and we have assumed toroidal symmetry so that $\partial D_r/\partial\phi \equiv 0$.

Since the wave phase velocity is much larger than the electron thermal speed we may use the cold plasma dispersion relation for D_r, Eq. (1). In (1) we now use for ω_p and ω_{ce} their local (r-dependent) values, set $S = k_\parallel c/\omega$, $k_\parallel = \mathbf{B}\cdot\mathbf{k}/B = (B_r k_r + B_\theta m/r + B_\phi\, n/R)B^{-1}$ with $\mathbf{B}(\mathbf{r})$ the equilibrium tokamak magnetic field, and $k_\perp^2 = k^2 - k_\parallel^2 = k_r^2 + (m/r)^2 + (n/R)^2 - k_\parallel^2$. The damping rate Γ is due to electron cyclotron resonance of the wave with particles satisfying the condition

$$\omega = k_\parallel v_\parallel + \omega_{ce}/\gamma_0$$

where γ_0 is he relativisic mass factor, $\gamma_0 = [1 - (v/c)^2]^{-1/2}$, v is the particle velocity and $v_\parallel = \mathbf{v}\cdot\mathbf{B}/B$. The calculation of Γ is straight-forward and is given in Appendix A.

To complete the formulation we need to specify the equilbrium magnetic field, **B**, plasma density, N, and electron temperature, T_e as functions of the coordinates r and θ. (We assume $T_e = T_i$ subsequently.) These are then substituted in the expressions for D_r and Γ to completely specify their spatial dependence. We assume that the toroidal component of **B** is a vacuum field, $B_\phi \sim R^{-1}$,

$$B_\phi = B_o[1 + \cos\theta(r/R_o)]^{-1}.$$

The other equilibrium quantities are obtained by considering a particular straight cylinder equilibrium and then making use of Shafranov's aspect ratio expansion[8] to obtain toroidal corrections to this equilibrium. Essentially, this gives a self-consistent toroidal equilibrium which is correct up to (and including) terms of order (r/R_o). For the straight cylinder we choose

$$N(r) = N(o)\,[1 - (r/a)^2]$$
$$B_\theta(r) = C_1(r/R_o)\; B_o[1 + C_2 r^2/a^2]^{-1},$$

where $r = a$ is the plasma edge, and C_1 and C_2 are constants. The details of the toroidal bending of the straight cylinder with these density and B_θ profiles are given in Ref. 6 and will not be repeated here.

B. Results and Dicussions

We have calculated the absorption properties of three different types of tokamaks: (A) "small size", an example is the Versator II (a = 11 cm, R_o = 40 cm) at the Massachusetts Institute of Technology; (B) "present-day size", an example is the Princeton Large Torus (a = 40 cm, R_o = 132 cm); and (C) "reactor size", an example is the UWMAK III (a = 270 cm, R_o = 810 cm), a conceptual reactor design done at the University of Wisconsin.[9]

In our calculations, the ordinary mode is always launched from the weak magnetic field side, while the extraodinary mode, is launched from the high field side (to avoid the cutoff). We also usually eschew launching the extraordinary mode at $\theta_o = 180°$ (where θ_o is the

poloidal angle at which the wave is launched, cf. Fig. 5) because the inside of the torus is usually occupied by transformers and other hardware, and, consequently, there is not much physical space available for wave launching structures. Instead, we shall usually take $\theta_o \sim 130°$.

For the extraordinary mode, the ray equations are solved until the ray reaches the upper hybrid resonance. At this point, the cold plasma approximation for D_r breaks down, and the calculation is stopped. As shown by Stix,[10] the extraordinary wave mode converts to a Bernstein wave at the upper hybrid resonance. The Bernstein wave will then propagate back into the region of increasing magnetic field. We have examined the propagation and absorption of Bernstein waves originating from the upper hybird resonance, and we have found that the waves propagate back toward the center of the torus and are typically fully absorbed shortly before they reach the cyclotron resonance.

The calculations which we present here are of most use when the launched ordinary or extraordinary wave is absorbed essentially completely in one pass through the center. As we shall see, this is typically the case for the larger, hotter tokamaks (e.g. Princeton Large Torus to reactor size), but not for smaller devices (e.g. Versator II). For the smaller devices, the full picture of extraordinary mode absorption involves the Bernstein wave mode conversion process discussed previously; while for the ordinary mode, reflections from the tokamak walls, and the limiter, etc., must be considered.

Type A Tokamaks

In Table I, we show the absorption of ordinary and extraordinary modes versus angle, density, temperature, and magnetic field for type A tokamaks (i.e. small size tokamaks). The definitions of symbols appearing in this table are as follows. θ_n denotes the poloidal angle location at which the wave is launched. ξ is the angle of incidence in the poloidal plane; i.e., the

angle between the projection of the launched wavenumber on the poloidal plane and a line joining the launch point with the point $r=0$. The definitions of the angles θ_o and ξ are shown in Fig. 5. The angle Θ specifies the ray direction at the launch point with respect to the toroidal direction,

$$\sin \Theta = (n/R)/(\omega/c)$$

where R is evaluated at the launch point. r_{max} is the radius of the magnetic surface where the energy deposition per unit volume averaged over a magnetic surface is maximum. Also, the symbols X and O in the table denote extraordinary and ordinary modes. We see from Table I that, for this type of tokamak, the absorption, in general, is small (due to the relatively low temperatures involved). While the density dependence for absorption is weak for the ordinary mode, it is strong for extraordinary mode. In fact, the extraordinary wave attenuation may be shown to be inversely proportional to density. The absorption for both modes does not vary much over a wide range of θ_o, except near $\theta_o = \pi/2$. If the angle θ_o approaches $\pi/2$ (i.e., the wave is launched close to the resonance), the energy is absorbed near the edge.

The angular dependence on Θ (which is a measure $k_{||}$) for the ordinary mode is also weak near $\Theta = 0$. The ordinary wave absorption decreases slowly as Θ increases. In contrast, the extraordinary mode absorption depends strongly on Θ, and increases as Θ increases, until the mode encounters the turning point X_2. We note that (from the small values of r_{max}/a in the table) for both modes most of the energy absorbed is deposited near the center.

The transmission profiles for the ordinary and extraordinary modes are plotted in Fig. 6 as a function x, where $x = -r\cos\theta$ (negative x corresponds to the weak field side). From the figure, we see that the profiles are very narrow and centered around $x = 0$.

A typical ray trajectory is shown in Fig. 7, where we plot the poloidal plane in the inner circle and the toroidal plane (a "top view" of the tokamak), in the outer circle.

Type B Tokamaks

The absorption parameters of type B tokamaks (e.g. the Princeton Large Torus) are shown in Table II. The dependence on Θ and θ_o are similar to that for type A tokamaks and will not be shown here. Here we are interested in the comparison between relativistic and non-relativistic absorption calculation, and the effect of a slight divergence of the incoming waves, i.e. $\xi \neq 0$ (see Fig. 5 for a pictorial definition of ξ).

Since all published calculations on electron cyclotron resonance absorption in tokamak geometry are nonrelativistic, it is of interest to compare nonrelativistic and relativistic calculations. From Table II, we see that relativity makes only a small difference for the ordinary mode, and the energy is essentially 100% absorbed near the center in both cases. However, there is a big difference for the extraordinary mode propagating at $\Theta = 0°$ and $\theta_o = 180°$. The nonrelativistic calculation predicts negligible absorption (because of the shear in magnetic field, k_{barbar} deviates slightly from zero as the mode propagates in, and the absorption is roughly 1%). On the other hand, the relativistic calculation for the same parametrers shows a 53% absorption. This is due mainly to the broadening of the cyclotron resonance through the energy dependence of the electron gyrofrequency. For $\Theta = 30°$ and $\theta_o = 125°$, we see that the extraordinary wave is fully absorbed in both the relativistic and nonrelativistic cases, but that the energy deposition profiles are quite different, cf. Fig. 8. This difference is enhanced in the reactor case (type C), as we shall see later.

In practice the heating waves will typically be launched from a horn antenna. Thus there will be some spectrum of launched wavenumbers (characterized by the antenna pattern). The range in angle of deviation ξ of the launched waves could be as large as $\pm$ 10°. Table II shows the results for $\xi = 0.5°$, 5° and 10°. From Fig. 9 and Table II we see that as the angular divergence increases, the mode deposits its energy farther and farther away from the center. Thus,

as a result of the spread in ξ, the composite energy deposition profile is considerably broadened.

The transmission profile of ordinary and extraordinary modes is shown in Fig. 10. Again we see that the profile is quite narrow, typically about 5% of the minor radius. Because of the high temperature ($\sim$ 3 KeV), the extraordinary mode usually does not deposit its energy very close to the center. A possible remedy for this is to tune the frequency slightly lower than the central cyclotron frequency. Such a case ($\omega = 0.9\ \omega^{\circ}_{ce}$) is shown in Figs. 10 (solid curve) and 11. We see that the maximum energy deposition is now at $r_{max}/a = 0.09$ instead of 0.33 (Table II).

Type C Tokamaks

The absorption characteristics of type C (reactor-size) tokamaks are shown in Table III. The difference between relativistic and nonrelativistic calculation is again very small for the ordinary mode. A blow-up of the transmission curve versus x is given in Fig. 12. For the extraordinary mode, however, the difference between relativistic and nonrelativistic calculations is significant. The energy deposition profiles and the transmission coefficient profiles for the extraordinary mode are given in Fig. 13 and Fig. 14. The effect of angular divergence, ξ, is rather strong. We show in Fig. 15 and Fig. 16 the results for $\xi = 0.5°$, 5° and 10°. Again it is evident that as ξ increases, (r_{max}/a) also becomes larger.

Finally, we study what happens to the absorption characterstics if we use electron cyclotron resonance heating to heat a reactor from an initial temperature of 2 KeV (such as would result from ohmic heating) to the ignition temperature, say 7 KeV. Blow-ups of the energy deposition curves and transmission coefficient profiles are shown in Fig. 17 and Fig. 18. We have partly optimized the heating by using $\omega = 0.95\ \omega^{\circ}_{ce}$. It is clear from Fig. 17 that the ener-

gy deposition profile becomes broader as the temperature increases, and the energy is deposited somewhat further from the center of the torus ($r_{max}/a = 0.02$ at T_e (0) = 2 KeV and $r_{max}/a = 0.28$ at $T_e(0) = 7$ KeV). Note that the launched waves are the same for Figs. 17 and 18, and that the results for both cases indicate wave absorption in the interior of the device. Thus these results indicate the possibility of heating to ignition *without* tuning the launched wave as the temperature rises.

Discussion

In concluding this section we note the following points:

(1) The one pass absorption is usually < 50% for small tokamaks (type A). However, for larger tokamaks (type B and type C), the absorption is usually essentially 100%.

(2) The energy absorption is usually in the interior of the device and can be further centered by tuning the frequency slightly lower than the central cyclotron frequency.

(3) Relativistic effects on the absorption coefficient can lead to significant differences (see also Fidone et al.[3]).

(4) Angular divergence of the launched waves shift the energy deposition profile.

(5) Heating of a tokamak reactor from an ohmically heated state to ignition without wave tuning is feasible.

(6) Since both the ordinary mode and the extraordinary mode are fully absorbed for type B and type C tokamaks, the choice between the two modes should depend on the availability of space (for the extraordinary mode), and the density requirements in conjunction with the accessibility condition. In particular, if we are interested in heating high density

tokamaks [$2 > (\omega_o/\omega_{ce}^{\circ})^2 > 1$], then the extraordinary mode is the only possible choice for the fundamental harmonic.

IV. SCATTERING BY DENSITY FLUCTUATIONS

In this section we consider the effect of low frequency density fluctuations (such as those that would be caused by drift waves) on the propagation of the externally launched heating wave. Strong scattering of the heating wave would substantially alter the picture of wave propagation and energy deposition which we have presented in the preceeding section.

To simplify the analysis we shall consider wave propagation *perpendicular* to $\mathbf{B}_o = B_o\mathbf{z}_o$ in a homogeneous medium. Since the frequency and parallel wave number of drift waves are low compared to the frequency and (perpendicular) wave number of the heating wave, we neglect them. Hence, on scattering, the wave frequency is conserved, and the propagation direction remains perpendicular to $\mathbf{B}_0$. Scattering of the direction of propagation in the plane perpendicular to $\mathbf{B}_0$, however, does occur.

First, we consider an ordinary mode heating wave, in which case the propagation is described by the following wave equation

$$\left\{\nabla_\perp^2 + \frac{\omega^2}{c^2} - \frac{\omega_p^2}{c^2}[1 + \delta n(\mathbf{r}_\perp)/N]\right\}E_z = 0, \tag{12}$$

where ω_p is the plasma frequency in the absence of fluctuations; N is the average electron density, and δn is the fluctuation in the electron density which depends on the position coordinates perpendicular to $\mathbf{B}_o$, $\mathbf{r}_\perp$. Fourier transforming (12) with respect to $\mathbf{r}_\perp$ we have

$$(-c^2k^2+\omega^2-\omega_p^2)E_{\mathbf{k}} = \omega_p^2 N^{-1}\sum_{\mathbf{k}'}\delta n_{\mathbf{k}'}E_{\mathbf{k}-\mathbf{k}'}$$

Replacing ω by $\omega^{(0)} + i\frac{\partial}{\partial t}$, where $[\omega^{(0)}]^2 = k^2c^2-\omega_p^2$, and expanding for $\omega^{(0)} >> \frac{\partial}{\partial t}$, we obtain the usual mode coupling equation

$$i\,\partial E_{\mathbf{k}}/\partial t = N^{-1}\sum_{k'} W\delta n_{\mathbf{k}'} E_{\mathbf{k}-\mathbf{k}'} \tag{13}$$

where the coupling coefficient W is given by

$$W \equiv \omega_p^2/(2\omega) \tag{14a}$$

which is independent of $\mathbf{k}$ and $\mathbf{k}'$ for the case under consideration. A similar, although algebraically more complicated calculation, also yields (13) for the extraordinary wave. For the case of the extraordinary wave W will in general depend on $\mathbf{k}$ and $\mathbf{k}'$. However, for the case of interest here ($\omega = \omega_{ce}$ in the center of the machine), $\omega \cong \omega_{ce}$ throughout the device. Adopting this approximation the expression for W simplifies (cf. Appendix B) and we obtain

$$|W| \cong [1 + (\omega_{ce}/\omega_p)^2]^{-1}\omega_p^2/(2\omega), \tag{14b}$$

for the extraordinary mode, which is independent of $\mathbf{k}$ and $\mathbf{k}'$. Applying the random phase approximation to the mode coupling equation, Eq. (13), and following Ref. 11, we have

$$\frac{dF}{dt} = 2\pi k |W|^2 v_g^{-1} \int_0^{2\pi} d\beta S[2k \sin(\beta/2)][F(\phi+\beta) - F(\phi)] \tag{15}$$

where $F(\phi)d\phi$ is the energy density of waves with wavenumber vectors whose angle to the x-axis is between ϕ and $\phi + d\phi$ so that the wave energy density is $\int_o^{2\pi} F(\phi)d\phi \cdot S(\kappa_\perp)$ denotes the two dimensional wavenumber spectrum of the low frequency density fluctuations (which are perpendicular to $\mathbf{B}_o$), defined so that the mean square relative density fluctuation level is

$$\langle (\delta n/N)^2 \rangle = \int_o^\infty S(\kappa_\perp) 2\pi\kappa_\perp d\kappa_\perp,$$

and we have assumed S to be isotropic (i.e. it depends only on $\kappa_\perp = |\kappa_\perp|$). We note that the integral operator on the right hand side of (15) has eigenfunction $\cos p\phi$ ($p = 0, 1, 2, \ldots,$) and eigenvalues $-\nu_p$:

$$\nu_p = 4\pi k |W|^2 v_g^{-1} \int_o^{2\pi} \sin^2(p\beta/2)\; S[2k \sin(\beta/2)]\; d\beta \tag{16}$$

As discussed in Ref. 11, a reasonable definition of the scattering length can be based on the damping (due to scattering) of the lowest order angular dependent eigenfunction ($p = 1$):

$$l_s = v_g/\nu_1. \tag{17}$$

To evaluate ν_1 we assume that $S(\kappa_\perp)$ is Gaussian (this is motivated by experiment, cf. Ref. 12)

$$S(\kappa_\perp) = \left\langle \left(\frac{\delta n}{N}\right)^2 \right\rangle \frac{1}{\pi \zeta_o^2} \exp\left(-\kappa_\perp^2/\zeta_o^2\right),$$

and $\zeta_o^2 \ll k^2$, in which case (16) becomes

$$\nu_1 \cong \frac{\sqrt{\pi}}{2} \frac{|W|^2 \zeta_o}{k^2 v_R} \langle (\delta n/N)^2 \rangle. \tag{18}$$

For drift waves, reasonable estimates of ζ_o and $\langle (\delta n/N)^2 \rangle$ which are consistent with some recent experiments on the PLT tokamak are[13]

$$\zeta_o \cong \rho_i^{-1} \text{ and } \langle (\delta n/N)^2 \rangle \cong (\zeta_o L_n)^{-2}, \tag{19}$$

where ρ_i is the ion gyro-radius and L_n is the density gradient scale length. (Note, however, that these estimates do not apply in all cases. In fact very large relative fluctuation levels have been observed on the Alcator tokamak[12].) From (14), (17) and (18)

$$l_s = 2(\pi)^{-1/2} [(k v_R)^2/|W|^2] (L_n/\rho_i)^2 \rho_i. \tag{20}$$

For $\omega \cong \omega_{ce}$ we have

$$k v_R \cong \omega_{ce} [2 - (\omega_p/\omega_{ce})^2] [1 + (\omega_{ce}/\omega_p)^2]^{-1} \tag{21a}$$

for the extraordinary wave and

$$k v_R \cong \omega_{ce} [1 - (\omega_p/\omega_{ce})^2] \tag{21b}$$

for the ordinary wave. For example, for the ordinary wave with $\omega_p^2/\omega_{ce}^2 \cong 1/2$, (14) (20) and (21) yield $l_s \sim 8 L_n^2/\rho_i$ which is typically very large. For the extraordinary wave with $\omega_p^2/\omega_{ce}^2 \cong 1$ we again obtain $l_s \sim 8 L_n^2/\rho_i$. The angular scattering of the propagation direction as the wave propagates from the edge to the center of the tokamak can be estimated on the basis that it is a diffusion process[11],

$$\Delta\phi \sim (a/l_s)^{1/2} \tag{22}$$

where a is the tokamak minor radius. Taking $L_n \sim a/2$ we obtain $\Delta\phi$ to be in the range 1° to 3° for PLT and reactor sized tokamaks. Thus we conclude that scattering should not be a problem, if the characteristics of the density flucutations are approximately consistent with (19).

V. PARAMETRIC INSTABILITIES

In this section we consider the possibility that the externally launched electron cyclotron resonant heating wave might produce parametric instabilities,[14] whereby its energy will feed into lower frequency decay waves. Our main result is that such parametric instabilties are unlikely under conditions that will apply in electron cyclotron resonance heating experiments in large tokamaks. This situation is in contrast with lower hybrid heating for which parametric instabilities are thought to be a definite problem. The reason for the greater stability in the case of electron cyclotron resonance heating can be crudely explained as follows. The strength of parametric instabilities depends on Δ, the displacement of a particle due to the action of the pump wave. For a lower hybrid (lh) pump, $\Delta^{lh} \sim E_o^{lh}/(B_o\, \omega_{lh})$, while for a pump with frequency near ω_{ce}, $\Delta^{ce} \sim E_o^{ce}/(B_o\, \omega_{ce})$, where E_o denotes the heating wave (pump) electric field amplitude. Furthermore, for a given input power flux density, P, the corresponding pump electric fields scale as $(E_o^{lh})^2 \sim P/v_{gr}^{lh}$ and $(E_o^{ce})^2 \sim P/v_{gr}^{ce}$ where v_{gr} is the radially inward component of the group velocity. Thus for fixed P, $(\Delta^{lh}/\Delta^{ce}) \sim (\omega_{ce}/\omega_{lh})\ (v_{gr}^{ce}/v_{gr}^{lh})^{1/2}$. Since $\omega_{ce}/\omega_{lh} \sim (m_i/m_e)^{1/2}$ and $v_{gr}^{ce} >> v_{gr}^{lh}$ we see that $(\Delta^{lh}/\Delta^{ce})$ is large. Hence lower hybrid waves might be expected to be much more susceptable to parametric instability processes. The preceeding arguement is too crude to be taken as a proof, but it does make our subsequent conclusions plausible.

If a window is used to isolate the wave generation region from the tokamak, then the heat loading which the window can tolerate sets an upper bound on the wave energy flux density. For continuous operation (i.e. times $\gtrsim$ 100 msec) the maximum power flux density which a window can withstand is[15] $\sim$ 10 kW/cm^2. Furthermore we note that this flux density should be quite adequate for heating a reactor plasma. For example, using numbers from the UWMAK III conceptual reactor design[9], we find that with an incident power flux density of 5 kW/cm^2

only about 0.1% of the available surface area need be utilized for heating ports. Thus if we find power flux density instability thresholds which greatly exceed 10 kW/cm^2 we shall conclude that parametric instabilities are unlikely in typical reactor situations.

We have considered parametric instabilities for cases in which the decay waves are electromagnetic and for cases in which the decay waves are electrostatic. We found that electromagnetic decays have much larger instability power flux density thresholds than do decays to electrostatic waves. The basic reason for this is that electromagnetic waves have large group velocities ($\sim c$), and hence rapidly convect out of the unstable region. We therefore limit the subsequent discussion to the slower moving electrostatic decay waves.

A. Propagation of Electrostatic Decay Waves in a Torus

In the frequency range around ω_{ce} there are two relevant types of electrostatic waves: cold plasma waves (i.e. the upper and lower hybrid wave branches) and the electron Bernstein waves. (In this section $(\hat{\omega}, \hat{\mathbf{k}})$ denote the frequency and wavenumber of a lower sideband electrostatic decay wave.) The cold plasma waves are characterized by $\hat{k}_\perp^2 \rho_e^2 << 1$ (where $\rho_e = v_e/\omega_{ce}$ is the electron Larmor radius and v_e is the electron thermal speed), and have dispersion relation

$$1 - \frac{\omega_{pe}^2}{\hat{\omega}^2 - \omega_{ce}^2}\frac{\hat{k}_\perp^2}{\hat{k}^2} - \frac{\omega_{pe}^2}{\hat{\omega}^2}\frac{\hat{k}_\parallel^2}{\hat{k}^2} - \frac{\omega_{pi}^2}{\hat{\omega}^2} = 0, \tag{23}$$

which can be solved for $\hat{k}_\perp^2$

$$\hat{k}_\perp^2 = \left(\frac{\omega_p^2}{\omega^2} - 1\right)\left(1 - \frac{\hat{\omega}_{pe}^2}{\hat{\omega}^2 - \omega_{ce}^2} - \frac{\omega_{pi}^2}{\hat{\omega}^2}\right)^{-1}\hat{k}_\parallel^2,$$

from which we see that propagation ($\hat{k}_\perp^2 > 0$) occurs in the ranges $\omega_{uh} > \hat{\omega} > \max(\omega_p, \omega_{ce})$ (the upper hybrid branch) and $\min(\omega_p, \omega_{ce}) > \hat{\omega} > \omega_{lh}$ (the lower hybrid or Gould-Trivelpiece branch) where $\omega_{uh}^2 = \omega_p^2 + \omega_{ce}^2$, $\omega_{lh}^2 = \omega_{pi}^2[1 + (\omega_p/\omega_{ce})^2]^{-1}$, and we have made use

of the approximation $m_e << m_i$. We take the heating wave frequency to match ω_{ce} in the center of the device. Thus if the magnitude of the equilibrium **B**-field scales approximately as R^{-1}, the surface where the decay wave frequency matches ω_{ce} must be at $R > R_o$ (note that the decay wave frequency must be less than the pump wave frequency). Thus we find that regions of propagation of cold plasma electrostatic decay waves are as shown in Fig. 19 for a low density case (i.e. $\omega_p^2 < \omega_{ce}^2$ everywhere), and in Fig. 20 for a high density case [$\omega_{po}^2 > (\omega_{ce}^o)^2$, where ω_{po} and ω_{ce}^o are ω_p and ω_{ce} evaluated at $r = 0$]. Note that the curves $\hat{\omega} = \omega_{ce}$ represent reflection surfaces for upper hybrid decay waves; the curves $\hat{\omega} = \omega_p$ represent reflection surfaces for lower hybrid decay waves; and the curves $\hat{\omega} = \omega_{uh}$ represent cold plasma resonances of the upper hybrid decay waves. To determine what happens at $\hat{\omega} = \omega_{ce}$ we plot the dispersion relation of the electron Bernstein mode ($\hat{k}_{\parallel} = 0$) in Fig. 21 for $\omega_{uh} < 2\omega_{ce}$ (i.e. $\omega_{pe}^2/\omega_{ce}^2 < 3$). We note that the Bernstein wave has a zero in $\hat{k}_{\perp}$ at the same place where the cold plasma wave has a resonance (namely $\hat{\omega} = \omega_{uh}$). Since Bernstein waves are short wavelength modes ($\hat{k}_{\perp} \rho_e \sim 1$ where the wave is in the center of the region $\omega_{uh} > \hat{\omega} > \omega_{ce}$), and cold plasma upper hybrid waves are long wave length modes ($\hat{k}_{\perp} \rho_e << 1$ in the center of the propagation region), we see that with finite $k_{\parallel}$ and T_e the cold plasma resonance becomes a mode conversion surface (cf. Stix[10]). Thus an upper hybrid mode traveling toward the $\omega = \omega_{uh}$ surface mode converts to an electron Bernstein wave which then travels back into the region of increasing magnetic field, eventually encountering a resonance at $\hat{\omega} = \omega_{ce}$ (this is evident from Fig. 21 which shows $\hat{k} \rightarrow \infty$ as $\hat{\omega} \rightarrow \omega_{ce}$). With regard to Figs. 19(c), 20(b) and 20(c), we note that the Gould-Trivelpiece waves are completely enclosed within reflection surfaces. Thus any Gould-Trivelpiece decay wave is forever confined within the high density region of the torus. Such decay waves could experience multiple interactions with the pump as they bounce around in their confined region and transit around in the toroidal direction.

B. Parametric Instability and Dispersion Relation

For the following discussion we use $(\Omega, \vec{\kappa})$ to denote the frequency and wavevector of the heating wave (pump) and $(\omega, \mathbf{k})$ for the frequency and wavevector of a parametrically distabilized low frequency perturbation, $\omega \ll \Omega$. The parametric dispersion relation for electrostatic waves in a magnetized plasma is (cf. Appendix C for a derivation)

$$\epsilon(\omega, \mathbf{k}) + |\mathbf{k} \cdot \Delta|^2 \epsilon_e(\omega, \mathbf{k})[1+\epsilon_i(\omega, \mathbf{k})] \left\{\frac{e_+^2}{\epsilon_+} + \frac{e_-^2}{\epsilon_-}\right\}, \tag{24}$$

where $\epsilon_\pm \equiv \epsilon(\omega \pm \Omega, \mathbf{k} \pm \vec{\kappa})$, $\epsilon = 1 + \epsilon_e + \epsilon_i$, ϵ_e and ϵ_i are the electron and ion dielectric constants, and $e_\pm$ is defined in Appendix C ($e_\pm = 1$ in the dipole approximation). For a pump electric field $\mathbf{E} = \mathbf{E}_0 \exp(-i\Omega t + i\vec{\kappa}\cdot\mathbf{x}) + (\text{complex conjugate})$, the quantity Δ given in Appendix C may be written

$$\Delta = \frac{-e}{m_e \Omega}\left\{z_o(E_{oz}/\Omega) + \mathbf{a}_+[E_+/(\Omega+\omega_c)] + \mathbf{a}_-[E_-/(\Omega-\omega_{ce}]\right\}, \tag{25}$$

where $E_\pm = (2)^{-1/2}(E_{ox} \mp i E_{oy})$, $\mathbf{a}_\pm = (2)^{-1/2}(\mathbf{x}_0 \mp i \mathbf{y}_0)$ and we have taken, $\mathbf{B}_0 = B_0 \mathbf{z}_o$. Note that for the stated definition of $\mathbf{E}_0$ the temporally averaged pump electric field, $\langle \mathbf{E}\cdot\mathbf{E} \rangle = 2\mathbf{E}_0\cdot\mathbf{E}_0^*$. As a point of reference we note that for an ordinary wave propagating nearly perpendicular to $\mathbf{B}_0 = B_0 \mathbf{z}_o$ $\vec{\kappa} = \kappa \mathbf{x}_0$ and $\Omega \approx \omega_{ce}$, we have

$$\begin{aligned} \mathbf{E}_0 &= E_0^o \mathbf{z}_o, \\ \Delta &= -cE_0^o \mathbf{z}_o/(B_0\Omega), \end{aligned} \tag{26a}$$

while for an extraordinary wave with $\vec{\kappa} = \kappa \mathbf{x}_0$ and $\Omega \approx \omega_{ce}$, we have

$$\begin{aligned} \mathbf{E}_0 &= E_0^x (i\mathbf{x}_0 + \mathbf{y}_0)/2^{1/2}, \text{ and} \\ \Delta &= cE_0^x[-i\,\Omega^2/\omega_p^2 \mathbf{x}_0 + (\Omega^2/\omega_p^2 - 1)\mathbf{y}_0]/(2^{1/2}B_0\Omega)\ . \end{aligned} \tag{26b}$$

Relating E_0^o and E_0^x to the time averaged poynting flux (P), we have from Maxwell's $\nabla \times \mathbf{E}$ equation,

$$E_0^o = (2\pi\Omega P/\kappa c^2)^{1/2} \quad \text{(ordinary mode)}, \tag{27a}$$

$$E_0^x = (4\pi\Omega P/\kappa c^2)^{1/2} \quad \text{(extraordinary mode)}. \tag{27b}$$

The two relevant types of parametric decay instabilities which we consider here are (1) the *nonresonant* decay of a pump $(\Omega,\vec{\kappa})$ to a lower frequency wave $(\omega-\Omega,\mathbf{k}-\kappa)$ by nonlinear Landau damping on particles satisfying $\omega=k_{||}v_{||}$; and (2) three wave *resonant* decay of the pump $(\Omega,\vec{\kappa})$ to a low frequency wave $(\omega,\mathbf{k})$, with $\Omega>>\omega$, and a lower sideband $(\omega-\Omega,\mathbf{k}-\vec{\kappa})$. (Nonlinear cyclotron damping at $\omega = k_{||}v_{||} + n\omega_{ce}$ is not considered).

We shall first, examine nonresonant decay instability. For nonresonant decay instabilities the wave propagation characteristics of the decay wave determine the threshold. For decay waves with growth rate γ and group velocity v_g we may define $k_i=\gamma/v_g$, the inverse exponentiation length. Then the total number of exponentiations of the decay wave as it convects through the unstable region occupied by the pump is $\int k_i dl$, where dl is a differential length along the ray path of the decay wave. A criterion for convective instability is then that the total number of exponentiations in the unstable region should be large. On the other hand, for decay waves which are trapped within a confined region (e.g. the region within $\omega_p>|\omega-\Omega|$ in Fig. 20), after a sufficient time, the decay wave sees an average of the growth rate over the confined volume. If this averaged γ is positive (i.e. the averaged parametric growth exceeds collisional and resonant particle damping), then an absolute instability results. Convective and absolute nonresonant instabilities will be discussed in Secs. VC and VD, respectively.

C. Nonresonant Decay to Electron Bernstein Waves

For nonresonant *convective* parametric decay the most dangerous mode is the electron Bernstein mode since its group velocity is much smaller than that for cold plasma waves. This in turn results in a larger k_i for Bernstein waves. Note that the Bernstein decay wave frequency is less than the frequency of the pump and hence only propagates on the low magnetic field

side of the surface where the pump frequency is equal to the cyclotron frequency. Since the extraordinary mode must be launched from the high magnetic field side of the torus, it will already have passed through its region of strong linear absorption before it can excite a Bernstein wave parametric instability. Thus this instability is primarily of interest for the ordinary wave.

To obtain an upper limit on $\int k_i dl$ we ignore the possiblity that the Bernstein wave may convect out of the pump region as it propagates. Thus we take the path integral from the upper hybrid resonant surface $\hat{\omega} = \omega_{uh}$ (more accurately the mode conversion layer) to the cyclotron resonance layer $\hat{\omega}=\omega_{ce}$ (cf. Fig. 20), where $\hat{\omega}\equiv\Omega-\mathrm{Re}(\omega)$. Since k_i becomes small at these end points we may roughly estimate $\int k_i dl$ as $k_i^o l_0$, where k_i^o is k_i in the middle of the region where the Bernstein wave propagates, and l_0 is the length of the ray path (roughly the distance between the $\hat{\omega}=\omega_{uh}$ surface and the $\hat{\omega}=\omega_{ce}$ surface). An upper bound on l_0 would be a, the minor radius. To estimate k_i, we expand the parametric dispersion relation for small k_i in the nonlinear Landau damping limit and obtain

$$k_i = -\left(\frac{\partial\epsilon_-}{\partial k_\perp}\right)^{-1} |\mathbf{k}\cdot\Delta|^2 \left[\frac{|1+\epsilon_i|^2}{|1+\epsilon_i+\epsilon_e|^2}\, Im(\epsilon_e) + \frac{|\epsilon_e|^2}{|1+\epsilon_i+\epsilon_e|^2}\, Im(\epsilon_i)\right], \tag{28}$$

where we have utilized $k >> \kappa$ appropriate for Bernstein waves and neglected linear damping processes. For nonlinear Landau damping on electrons the expression for k_i can be written

$$k_i\rho_e = \left(\frac{\partial\epsilon_-}{\partial\lambda}\right)^{-1} \hat{\xi}|\mathbf{k}\cdot\Delta|^2, \tag{29}$$

where

$$\lambda = k_\perp\rho_e ,$$
$$\hat{\xi} = -|1+\epsilon_i|^2\,|1+\epsilon_i+\epsilon_e|^{-2}\,\mathrm{Im}(\epsilon_e) ,$$
$$\mathrm{Im}(\epsilon_e) = \pi\, I_0(\lambda^2)\exp(-\lambda^2)\lambda^{-2}\omega_{pe}^2\omega_{ce}^{-2}v_R F_0(v_R) ,$$
$$F_0(v) = (2\pi v_e^2)^{-1/2}\exp-(v^2/2v_e^2) ,$$

and

$$v_R=(\Omega-\hat{\omega})/k_{\parallel} .$$

Maximizing $\hat{\xi}$ we have $\hat{\xi} \sim 0.35$. For a point in the middle of the unstable region $\lambda \sim 1$ and $(\partial\epsilon_-/\partial\lambda)\sim 1$ for $\omega_{pe}^2/\omega_{ce}^2 \sim 1$. Thus, using $\int k_i dl \gtrsim 10$ and $l_o \sim a$, we obtain the following estimate of the instability threshold

$$|\mathbf{k}\cdot\Delta|^2 \gtrsim 30(\rho_e/a) . \tag{30}$$

Using $\Omega/\kappa \sim c$, $\Omega \sim \omega_{ce} \sim \omega_{pe}$, $\Delta \sim (B_o\,\omega_{ce})^{-1}(2\pi P)^{1/2}$, and Eqs. (26b) and (27b), with $\lambda = 1$, Eq. (30) can be rewritten as

$$P_0 \sim 2\times 10^4 \frac{kW}{cm^2}\left[\left(\frac{N}{10^{14}cm^{-3}}\right)^{1/2}\left(\frac{T_e}{10keV}\right)^{3/2} a^{-1}\right], \tag{31}$$

where a is in meters, and P_o is the threshold power flux density. (Recalling that our estimates have generally favored instability, we expect P_0 to actually be underestimated by (31).) Thus, if as previously stated, P is limited to about 10kW/cm^2, we see that P_0 is far too high for this parametric process to occur.

D. Absolute Parametric Instability

For waves which are trapped within the interior of the torus [e.g. Fig. 19(c)] an absolute instability is possible if the average parametric growth along the ray path exceeds the average collisional and resonant particle damping. We can define the temporal averaged growth rate as

$$\langle\gamma\rangle \equiv \lim_{t\to\infty}\left\{t^{-1}\int_0^t \gamma[\mathbf{r}(t),\,\mathbf{k}(t)]\,dt\right\},$$

where the evolution of $\mathbf{r}$ and $\mathbf{k}$ is obtained from the ray equations. Instability occurs if $\langle\gamma\rangle$ is positive (cf. Appendix D). (We shall use the dipole approximation so that no distinction

between $\mathbf{k}$ and $\hat{\mathbf{k}}$ is necessary.) It is reasonable to assume that due to the poloidal dependence of the equilibrium quantities, there is no constant of the ray motion analogous to rk_θ (which is a constant of the motion for the straight cylindrical case). In such a case we may make use of the Hamiltonian form of ray equations to infer that the ray wanders ergodicly over all regions of phase space (i.e. $\mathbf{r}-\mathbf{k}$ space) that are allowed by the constants of the motion $\hat{\omega}$ and $n = Rk_\phi$ ($\hat{\omega}$ is constant because the equilibrium is time independent and n is constant because of toroidal symmetry). In fact the ergodic wandering of rays due to toricity of the equilibrium has been explicitly demonstrated for a case involving lower hybrid waves (cf. Ref. 6 which also includes further discussion of ray ergodicity). Thus the ergodic theorem may be utilized to convert $<\gamma>$ from a time integral to an integral over phase space (i.e. $\mathbf{r}$, $\mathbf{k}$ space),

$$<\gamma> = \frac{\int \gamma(\mathbf{r},\mathbf{k})\,\delta[\hat{\omega}-\hat{\omega}(\mathbf{r},\mathbf{k})]\,\delta[k_\phi-(n/R)]\,d\mathbf{r}d\mathbf{k}}{\int \delta[\hat{\omega}-\hat{\omega}(\mathbf{r},\mathbf{k})]\,\delta[k_\phi-(n/R)]\,d\mathbf{r}d\mathbf{k}}, \tag{32}$$

where $\hat{\omega}=\Omega-\mathrm{Re}(\omega)$ is the decay wave frequency with $\hat{\omega}(\mathbf{r},\mathbf{k})$ a solution of (23), and δ (...) denotes the delta function.

Again making the electron nonlinear Landau damping and the dipole approximation in (24) we obtain the temporal growth rate

$$\gamma = \left(\frac{\partial \epsilon_-}{\partial \omega}\right)^{-1} [|\mathbf{k}\cdot\Delta|^2\hat{\xi} - Im(\epsilon_-)] \,. \tag{33}$$

The term $|\mathbf{k}\cdot\Delta|^2\hat{\xi}$ represents parametric growth [cf. Eq. (29) for the definition of $\hat{\xi}$] and is counteracted by the linear damping term $Im(\epsilon_-)$. For $Im(\epsilon_-)$ we utilize the collisonal contribution only, since the resonant particle damping at $\hat{\omega}=k_\parallel v_\parallel$ may be made small by making $\hat{\omega}/k_\parallel >> v_e$:

$$Im(\epsilon_-) \cong \frac{\nu}{\hat{\omega}} \left[\left(\frac{k_\parallel}{k}\right)^2\left(\frac{\omega_p}{\hat{\omega}}\right)^2 + \left(\frac{k_\perp}{k}\right)^2 \frac{\omega_p^2}{\hat{\omega}^2-\omega_{ce}^2}\cdot\frac{\hat{\omega}^2+\omega_{ce}^2}{\hat{\omega}^2-\omega_{ce}^2}\right],$$

where ν is the electron-ion collision frequency, and $\nu/\hat{\omega} << 1$ is assumed. From (33) and the

assumed ergodicity of the decay wave ray trajectory, we obtain the instability condition

$$<|\mathbf{k}\cdot\Delta|^2\hat{\xi}> \gtrsim <\mathrm{Im}(\epsilon_-)> , \tag{34}$$

which follows from $<\gamma> > 0$. Again we utilize rough estimates to obtain an idea of whether the existance of such an instability is plausible. Taking $\hat{\xi}\sim 0.35$ (its maximum value), $\Delta^2\sim(B_0\omega_{ce})^{-2}2\pi Pc$, $\omega_{ce}^2\sim\omega_{pe}^2$ and $\mathrm{Im}(\epsilon_-)\sim\nu/\omega_{pe}$, we obtain the instability condition $<P> \gtrsim 5.7(N T_e c)(\nu/\omega_p)(k\rho_e)^{-2}$, which with, $\nu \cong 3\times10^{-6}\, N\lambda T_e^{-3/2}$ (where N is in cm^{-3}, T_e is in eV, and λ is the usual Coulomb logarithm $\lambda\sim15$) yields the threshold power flux averaged over the plasma volume

$$<P>_0 \sim 2.2\frac{kW}{cm^2}\left(\frac{10keV}{T_e}\right)^{1/2}\left(\frac{N}{10^{14}cm^{-3}}\right)^{3/2}\left(\frac{0.1}{k^2\rho_e^2}\right)$$

Recalling that $k^2\rho_e^2 << 1$ for the validity of (23) we see that $k^2\rho_e^2 \sim 0.1$ is a reasonable upper bound. Also assuming that heating ports take no more than one percent of the tokamak wall area, we have $P \gtrsim 10^2<P>$. Thus P_o, the threshold power flux density, satisfies

$$P_0 \gtrsim (220\ kW/cm^2)\ (10keV/T_e)^{1/2}[N/(10^{14}cm^{-3})]^{3/2} , \tag{35}$$

and again we see that P_0 is too large for instability to occur in typical situations for a tokamak reactor. In extreme conditions for a present-day lower density device the instability might be possible. For example, with $P=5\,kW/cm^2$, $T_e=1keV$, instability occurs for $N \lesssim 4\times10^{12}\ \mathrm{cm}^{-3}$.

E. Resonant Decay to an Ion Cyclotron Wave and a Cold Plasma Wave

The wave number of the pump satisfies $\kappa \sim \omega_{ce}/c$. The frequency of the cold plasma decay wave is slightly (by about ω_{ci}) below the pump frequency; so it too is of order ω_{ce}. Since the cold plasma wave is electrostatic, we assume that its phase velocity is much less than c, i.e.

$$\omega_{ce}/k << c \sim \omega_{ce}/\kappa.$$

Thus we have $k >> \kappa$. This justifies the use of dipole approximation. Furthermore, we can

write

$$\kappa\rho_i \sim \omega_{ce} v_i/(\omega_{ci} c) = 1.9(m_i/m_p)^{1/2}\ T_i^{1/2}(keV)\ ,$$

where m_p is the mass of a proton. Since $k >> \kappa$, we have

$$k\rho_i >> 1.9\ (m_i/m_p)^{1/2}\ T_i^{1/2}(keV)\ .$$

Thus, for $T_i \gtrsim 200\ m_i/m_p\ eV$, we have

$$k^2\rho_i^2 >> 1\ ,$$

and $\epsilon = 1+\epsilon_e+\epsilon_i$ for the ion cyclotron wave can be written

$$\tilde{\epsilon} = 1+k^{-2}\lambda_{De}^{-2} - \omega_{pi}^2\ \omega_{ci}/[(2\pi)^{1/2}k^3\rho_i\ v_i^2(\omega-\omega_{ci})]\ . \tag{36}$$

Since the decay occurs for ion cyclotron waves which have $k_\parallel^2 << k^2$ and, since the dipole approximation is valid, the wavenumber of the high frequency decay wave is also almost perpendicular to **B**. This implies that the high frequency decay wave is an upper hybrid wave existing near the upper hybrid resonance surface, which is toward the plasma edge on the low magnetic field side of the tokamak. Thus, this decay process is unimportant for an extraordinary wave which must be launched from the high magnetic field side and propagate through the resonant absorption region ($\omega \approx \omega_{ce}$) before it reaches the region where this process can occur. Hence, we only consider this process for an ordinary wave.

For a three wave decay instability, the parametric dispersion relation [Eq. (24)] in the dipole approximation reduces to

$$\epsilon\epsilon_- + |\mathbf{k}\cdot\Delta|^2\epsilon_e(1+\epsilon_i) = 0\ , \tag{37}$$

where ϵ_- is given by (for $k^2\rho_e^2 << 1$)

$$\epsilon_- = 1+\epsilon_\perp k_\perp^2/k^2 + \epsilon_\parallel\ k_\parallel^2/k^2, \tag{38}$$

with $\epsilon_\perp = -\omega_{pe}^2/(\hat{\omega}^2-\omega_{ce}^2)$ and $\epsilon_\parallel = -\omega_{pe}^2/\hat{\omega}^2$. By Taylor expansion of Eq. (37), we obtain

$$\frac{\partial\epsilon_-}{\partial\hat{\omega}}\ \frac{\partial\epsilon}{\partial\omega}\ \gamma^2 = -\ |\mathbf{k}\cdot\Delta|^2\epsilon_e\ (1+\epsilon_i)\ , \tag{39}$$

where $\gamma = \mathrm{Im}(\omega)$.

The quantity of interest is

$$\hat{\eta} \equiv \gamma^2 / | v_{gx} v_{gx-} \frac{d}{dx} [k_x(x) - k_{x-}(x)] | , \tag{40}$$

where the minus subscript refers to the lower sideband (upper hybrid) wave. In terms of $\hat{\eta}$, the instability threshold criterion is $\hat{\eta} > 1$ (cf. Rosenbluth[16]). Inserting the expression for γ^2 obtained from Eq. (39) into Eq. (40), and applying the relations $v_{gx} = \partial\omega/\partial k_x = -(\partial\epsilon/\partial k_\perp)(\partial\epsilon/\partial\omega)^{-1} k_x/k_\perp$, $\epsilon_e = -1 - \epsilon_i \cong k^2 \lambda_{De}^2$, we obtain

$$\hat{\eta} = \frac{|k_\perp/k_x| \, |\mathbf{k}\cdot\Delta|^2}{k^4 \lambda_{De}^4 \, | \frac{\partial\epsilon_-}{\partial k_\perp} \frac{\partial\epsilon}{\partial k_\perp} \frac{d}{dx}(k_{\perp-} - k_\perp) |} . \tag{41}$$

From Eqs. (36) and (38), we obtain

$$\partial\epsilon_-/\partial k_\perp = -2k_\perp k_\parallel^2 (1+\epsilon_\parallel)/k^4 , \tag{42}$$

$$\partial\epsilon/\partial k_\perp = (k_\perp^3 \lambda_{De}^2)^{-1} , \tag{43}$$

$$\frac{d}{dx}(k_{\perp-} - k_\perp) = \frac{k_\perp^3}{2k_\parallel^2} \frac{d\epsilon_\perp/dx}{1+\epsilon_\parallel} - k_\perp^2 \rho_i (2\pi)^{1/2} \frac{Ti}{Te} \frac{1}{\omega_{ce}} \frac{d\omega_{ce}}{dx} , \tag{44}$$

where

$$d\epsilon_\perp/dx = -\omega_{pe}^{-2} (d\omega_{pe}^2/dx + d\omega_{ce}^2/dx) . \tag{45}$$

We observe from Eqs. (43) and (44) that $d(k_{\perp-} - k_\perp)/dx$ cannot be made zero in the region of interest (i.e. the low magnetic field side of the tokamak), where all the terms on the right hand side of Eq. (44) have the same sign. We also observe from Eqs. (41)-(44) that $\hat{\eta}$ maximizes at small $k_\parallel$ so that the second term on the right hand side of Eq. (44) can be neglected. Thus, combining Eqs. (41)-(44), we obtain the following threshold criterion for the instability

$$\hat{\eta} \approx | \frac{k_\perp}{k_x} | \frac{|\mathbf{k}\cdot\Delta|^2}{k^2 \lambda_{De}^2} \frac{k}{|d\epsilon_\perp/dx|} \gtrsim 1 . \tag{46}$$

To evaluate $\hat{\eta}$ numerically, we note that, for small angles (θ_i) between $\vec{\kappa}$ and the magnetic

field, $|\mathbf{k}\cdot\Delta|^2 = k^2\Delta^2 \sin^2\theta_i = k^2\Delta^2\theta_i^2$ for an ordinary wave. From Eq. (45), we can approximate $d\epsilon_\perp/dx$ by a^{-1}, where a is the plasma radius. Thus, Eq. (46) can be expressed

$$\hat{\eta} = \left|\frac{k_\perp}{k_x}\right| \sin^2\theta_i \frac{\omega_{pe}^2}{\omega_{ce}^2} \frac{\Delta^2}{\rho_e^2} ka \gtrsim 1 \tag{47}$$

Since the wave frequency is approximately the upper hybrid frequency at the instability point and the cyclotron frequency in the center, we have $\omega_{pe}^2 + \omega_{ce}^2(1-r/R) \simeq \omega_{ce}^2$. Hence $\omega_{pe}^2/\omega_{ce}^2 \simeq 2r/R$ and Eq. (47) can be written

$$\hat{\eta} = 2\left|\frac{k_\perp}{k_x}\right| \theta_i^2 \frac{r}{R} \frac{\Delta^2}{\rho_e^2} ka \gtrsim 1 \,. \tag{48}$$

Substituting $\Delta^2 = 2\pi\, P\, c/B_o^2\omega_{ce}^2$ into Eq. (48), we obtain the instability condition,

$$\hat{\eta} = 0.28\left|\frac{k_\perp}{k_x}\right| \frac{r}{R}\theta_i^2 k\rho_e \frac{P(kW/cm^2)\,a(m)}{B(T)\; T_e^{3/2}(keV)} \gtrsim 1 \,. \tag{49}$$

For example, with $k\rho_e < 1$, $r/R < 0.2$, $\theta_i < 0.3$ (about 10°), Eq. (49) yields

$$P \gtrsim (200\ kW/cm^2)\,|k_x/k_\perp|\; B_o\, T_e^{3/2}\, a^{-1}. \tag{50}$$

with B_o, T_e and a in tesla, keV and meters, respectively. Equation (50) shows that, except for $|k_x/k_\perp| \lesssim 10^{-2}$ (side-scattering), this instability would not take place. The case of side-scattering requires a more involved analysis along the lines of Ref. 17 which we defer for further study.

VI. CONCLUSIONS

Neither parametric instability nor scattering by existing density fluctuations appear to be serious problems for heating tokamaks by the electron cyclotron resonance. The accessibility conditions *do* impose serious limitations on the maximum density that can be heated. However, beta limitations on stability may result in tokamak parameters consistent with the accessibility requirements. (The acessibility condition is further relaxed for 2 ω_{ce} heating, which we shall

discuss in a future publications[21].) The predictions of a linear ray trajectory code have shown that for large tokamaks the wave energy absorption is essentially complete on one pass, and that this absorption is in the plasma interior. Furthermore, it appears feasible to heat a reactor plasma from an ohmically heated state to ignition without wave tuning. In addition, by properly launching the heating wave, it may be possible to attain a degree of control over the energy deposition profile (this may be desirable in order to eliminate desruptions due to internal kinks). We emphasize that these linear predictions should be accurate in the light of our tentative findings that parametric instabilities and scattering are unimportant. Thus we conclude that, subject to uncertainties in the lutimate development of gyrotron wave sources and in the stable beta limit, electron cyclotron resonance heating has many favorable features which make it attractive for tokamak applications.

ACKNOWLEDGMENTS

We wish to thank J.-M. Wersinger, T. Antonsen, V. L. Granatstein, for discussion.

This work was supported by the Department of Energy.

Appendix A

THE LINEAR DISPERSION RELATION

The conditon for electron cyclotron resonance is

$$\omega - k_{\parallel} v_{\parallel} - \omega_{ce}/\gamma_o = 0 \,. \tag{A.1}$$

It can be shown that if

$$k_{\parallel} c/\omega_{ce} < v_e/c \,, \tag{A.2}$$

where v_e is the electron thermal speed, the third term in (A.1) is a more sensitive function of electron thermal spread than the second term. [Equation (A.2) can also be written, $\hat{\Theta} \lesssim 2.7\,°T_e^{1/2}$, with T_e in keV where $\sin \hat{\Theta} = k_{\parallel} c/\omega$.] Since variation of the third term is caused by the relativistic factor γ, it is expected that under condition (A.2) the relativisitc effect will play an important role in the wave-electron resonance. Therefore, to obtain a general formulation, one needs to employ the relativistic Vlasov equation and the full set of Maxwell equations. Letting $\mathbf{k} = k_{\perp}\, \mathbf{e}_x + k_{\parallel}\, \mathbf{e}_{\parallel}$, and assuming a Maxwellian electron distribution,

$$f_o = (2\pi)^{-3/2} \theta_e^{-3} \exp[-p^2/2\theta_e^2] \,,$$

where p is the momentum and $\theta_e \equiv m_e v_e$, we have derived the following dispersion relation after some standard algebraic manipulations[18].

$$D = \det|d_{ij}| = 0, \tag{A.3}$$

where

$$d_{xx} = 1 - k_{\parallel}^2 c^2/\omega^2 + \sum_n n^2 m_e^2 \omega_p^2 \omega_{ce}^2 < J_n^2(\lambda) > /\theta_e^2 k_{\perp}^2 \omega \,,$$

$$d_{yy} = 1 - k_{\parallel}^2 c^2/\omega^2 + \sum_n \omega_p^2 < p_{\perp}^2 J_n'^2(\lambda) > /\theta_e^2 \omega \,,$$

$$d_{zz} = 1 - k_\perp^2 c^2/\omega^2 + \sum_n \omega_p^2 < p_\parallel^2 J_n^2(\lambda) > /\theta_e^2 \omega ,$$

$$id_{xy} = -id_{yx} = \sum_n n m_e \omega_p^2 \omega_{ce} < p_\perp J_n(\lambda) J_n'(\lambda) > /\theta_e^2 k_\perp \omega ,$$

$$d_{xz} = d_{zx} = k_\perp k_\parallel c^2/\omega^2 + \sum_n n m_e \omega_p^2 \omega_{ce} < p_\parallel J_n^2(\lambda) > /\theta_e^2 k_\perp \omega ,$$

$$id_{yz} = -id_{zy} = -\sum_n \omega_p^2 < p_\perp p_\parallel J_n(\lambda) J'_n(\lambda) > /\theta_e^2 \omega ,$$

$$\lambda = k_\perp p_\perp / m_e \omega_{ce} ,$$

$$J'_n(\lambda) = dJ_n(\lambda)/d\lambda ,$$

$$< G > \equiv 2\pi \int_0^\infty p_\perp dp_\perp \int_{-\infty}^\infty dp_\parallel \frac{f_o G}{k_\parallel p_\parallel / m_e + n\ \omega_{ce} - \gamma\omega} . \qquad \text{(A.4)}$$

To evaluate integrals of the form (A.4), we assume $\lambda << 1$ and expand the Bessel funtions in terms of λ. Note that Landau path is implicit in the $p_\parallel$-integration. To lowest order in λ, we obtain the cold plasma dispersion relation [Eq. (1) of the main test]. To next order in λ, there are two types of contributions to the integral. The resonant electrons give rise to the imaginary part of $< G >$ (through the residue of the poles) and consequently cause the wave to damp. The nonresonant electrons only add an insignificant contribution to the real part of $< G >$. For the present study, we will neglect these (higher order) nonresonant electron contributions. After some algebra, we obtain the final expressions for the d_{ij}'s,

$$d_{xx} = 1 - k_\parallel^2 c^2/\omega^2 - \omega_p^2/(\omega^2 - \omega_{ce}^2) + i\ (2\pi)^{1/2} \omega_p^2 m_e c\ I(0)/8\theta_e^5 \omega ,$$

$$d_{yy} = 1 - k^2 c^2/\omega^2 - \omega_p^2/(\omega^2 - \omega_{ce}^2) + i(2\pi)^{1/2}\ \omega_p^2 m_e c I(0)/8\theta_e^5 \omega ,$$

$$d_{zz} = 1 - k_\perp^2 c^2/\omega^2 - \omega_p^2/\omega^2 + i(2\pi)^{1/2} \omega_p^2 k_\perp^2 c\ I(2)/8\theta_e^5 \omega m_e \omega_{ce}^2 ,$$

$$id_{xy} = -id_{yx} = -\omega_{ce}\omega_p^2/\omega(\omega^2 - \omega_{ce}^2) + i(2\pi)^{1/2} \omega_p^2 m_e c\ I(0)/8\theta_e^5 \omega$$

$$d_{xz} = d_{zx} = k_\parallel k_\perp c^2/\omega^2 + i(2\pi)^{1/2}\ \omega_p^2\ k_\perp c\ I(1)/8\theta_e^5 \omega\ \omega_{ce} ,$$

$$id_{yz} = -id_{zy} = -i(2\pi)^{1/2} \omega_p^2 k_\perp c\ I(1)/8\theta_e^5 \omega \omega_{ce} ,$$

where

$$I(s) = \int_0^{p_{\perp m}} p_\perp^3 F(s, p_\perp)\ dp_\perp ,$$

$$F(s,p_\perp) = [(1 + p_\perp^2/m_e^2 c^2)(k_\parallel^2 c^2 - \omega^2) + \omega_{ce}^2]^{-1/2}$$

$$\times \{\gamma_- p_{\parallel -}^2 \exp[-(p_\perp^2 + p_{\parallel -}^2)/2\theta_e^2] + \hat{\Theta}\gamma_+ P_{\parallel +}^2 \exp[-(p_\perp^2 + p_{\parallel +}^2)/2\theta_e^2]\},$$

$$P_{\parallel \pm} = m_e c\ (\omega^2 - k_\parallel^2 c^2)^{-1} \{k_\parallel c \omega_{ce} \pm \omega[(1 + p_\perp^2/m_e^2 c^2)(k_\parallel^2 c^2 - \omega^2) + \omega_{ce}^2]\},$$

$$\gamma_\pm = [1 + (p_\perp^2 + p_{\parallel \pm}^2)/m_e^2 c^2] ,$$

$$p_{\perp m} = \begin{cases} Re\ \{m_e c[\omega_{ce}^2/(\omega^2 - k_\parallel^2 c^2) - 1]^{1/2}\}\ ) & \text{if } \omega/k_\parallel > c, \\ \infty\ , & \text{if } \omega/k_\parallel < c, \end{cases}$$

and

$$\hat{\theta} = \begin{cases} 1\ , & \text{if } \omega/k_\parallel > c\ , \\ 0\ , & \text{if } \omega/k_\parallel < c\ . \end{cases}$$

Appendix B

CALCULATION OF W FOR THE EXTRAORDINARY MODE

From Maxwell's equations we have

$$\nabla\times\nabla\times \mathbf{E} - \frac{\omega^2}{c^2}E = \frac{-4\pi i\omega}{c^2}(N+\delta n)e\,\underset{\sim}{\mu}\cdot\mathbf{E},$$

where $\underset{\sim}{\mu}$ is the mobility tensor

$$\underset{\sim}{\mu} = c\omega_{ce}\,[B_0(\omega_{ce}^2-\omega^2)]^{-1}\,[i\,(\omega-\omega_{ce})\,z_0\times]\,\underset{\sim}{I},$$

where $\underset{\sim}{I}$ is the unit tensor and we have assumed that $\mathbf{E}$ is perpendicular to $\mathbf{B}_0$ and has time dependence $\exp(-i\omega t)$. Fourier transforming in space we have

$$\left[-\mathbf{k}\times\mathbf{k}\times\underset{\sim}{I} - \frac{\omega^2}{c^2}\,\underset{\sim}{I} + \frac{4\pi i\omega Ne}{c^2}\underset{\sim}{\mu}\right],\ \mathbf{E}_{\mathbf{k}} = -\frac{4\pi i\omega e}{c^2}\underset{\sim}{\mu}\cdot\sum_{\mathbf{k}'}\delta n_{\mathbf{k}-\mathbf{k}'}\,\mathbf{E}_{\mathbf{k}'}. \qquad \text{(B-1)}$$

With $\delta n\to 0$, Eq. (B-1) yields the well-known properties of the linear extraordinary mode propagating in a homogeneous medium: the dispersion relation is

$$D(k,\omega) = k^2 - \frac{\omega^2}{c^2} + \frac{\omega_p^2}{c^2}\,\frac{\omega^2-\omega_p^2}{\omega^2-\omega_p^2-\omega_{ce}^2} = 0,$$

and the polarization vector (a unit vector in the direction of $\mathbf{E}$) is

$$\mathbf{e}_0 = (1+\rho^2)^{-1/2}\,[\mathbf{y}_0 + i\rho\mathbf{x}_0]\ ,$$

for wave propagation in the x direction, and

$$\rho = \omega^{-1}\omega_{ce}\omega_p^2(\omega_p^2+\omega_{ce}^2-\omega^2)^{-1}.$$

Note that for $\omega \cong \omega_{ce}$, $\rho \cong 1$ and $\mathbf{e}_o \cong (2)^{-1/2}\,(\mathbf{y}_0 + i\mathbf{x})$. Let $\mathbf{e}_\mathbf{k}$ denote the polarization vector for a wave propagating in some arbitrary direction $\mathbf{k} = (k\cos\beta,\ k\sin\beta)$, then $\mathbf{e}_\mathbf{k} = \mathbf{R}\cdot\mathbf{e}_0$ where $\mathbf{R}$ is the rotation matrix

$$\mathbf{R} = \begin{bmatrix} \cos\beta & -\sin\beta \\ \sin\beta & \cos\beta \end{bmatrix}.$$

Dotting (B-1) with $\mathbf{e}_\mathbf{k}^*$ we obtain

$$D(k,\omega)\ E_\mathbf{k} = -(1+\rho^2)4\pi i\omega e c^{-2} \sum_{\mathbf{k}'} \mathbf{e}_\mathbf{k}^* \cdot \underset{\sim}{\mu} \cdot \mathbf{e}_{\mathbf{k}'}\ \delta n_{\mathbf{k}-\mathbf{k}'} E_{\mathbf{k}'} \,. \tag{B-2}$$

where we have used $\mathbf{E}_\mathbf{k} \equiv \mathbf{e}_\mathbf{k} E_\mathbf{k}$. As for the ordinary mode case, we replace ω by $\omega^{(0)} + i\partial/\partial t$, $D(\omega^{(0)},\ k) \equiv 0$, and expand (B-2) for $\omega^{(0)} >> \partial/\partial t$. The result is the mode coupling equation, Eq. (13), with W now given by

$$W = -\left(\frac{\partial D}{\partial \omega}\right)^{-1} (1+\rho^2)\ 4\pi i\omega c^{-2} Ne\ \mathbf{e}_\mathbf{k}^* \cdot \underset{\sim}{\mu} \cdot \mathbf{e}_{\mathbf{k}'} \,. \tag{B-3}$$

For $\omega = \omega_{ce}$ this expression for W yields (after some algebra)

$$W = \frac{\omega_p^2}{2\omega}\left[1+\frac{\omega_{ce}^2}{\omega_p^2}\right]^{-1}\left[\cos(\beta'-\beta) + i\sin(\beta'-\beta)\right], \tag{B-4}$$

which gives Eq. (14b).

Appendix C

PARAMETRIC DISPERSION RELATION FOR ELECTROSTATIC DECAY WAVES IN A MAGNETIZED PLASMA

In this appendix we use the ponderomotive potential method[19] together with the expression for the ponderomotive force in a *magnetized* plasma[20] to derive the parametric dispersion relation for electrostatic waves. (The dipole approximation is not necessary and is not used in what follows.)

Let $\phi_\pm$ and $\delta n^\pm$ denote high frequency potential and *second order* parts of the electron density perturbations at ($\omega \pm \Omega$ and $\mathbf{k} \pm \vec{\kappa}$). Let ϕ' and $\delta n_e'$ be low frequency potential and electron density perturbation at (ω, $\mathbf{k}$). Let $\mathbf{E}_0$ denote the complex pump electric field amplitude such that the actual pump field is $\mathbf{E}_0 \exp(-i\Omega t + i\vec{\kappa} \cdot \mathbf{x})$ + (complex conjugate).

a. *High frequency components*: From Poisson's equation and the definition of the plasma dielectric constant

$$(\mathbf{k} \pm \kappa)^2 \epsilon_\pm \phi^\pm = -4\pi Ne(\delta n^\pm / N) \tag{C-1}$$

where $\epsilon_\pm = \epsilon(\omega \pm \Omega, \mathbf{k} \pm \kappa)$ are the dielectric functions for waves with frequencies $\omega \pm \Omega$ and wavenumber $\mathbf{k} \pm \kappa$. From the continuity equation and the cold plasma electron momentum equation we obtain

$$4\pi(\omega \pm \Omega) e\delta n^\pm \pm i \frac{\omega_p^2}{\Omega} (\mathbf{k} \pm \vec{\kappa}) \cdot \begin{Bmatrix} \underset{\sim}{\chi}(\Omega) \cdot \mathbf{E}_o \\ \underset{\sim}{\chi}^*(\Omega) \cdot \mathbf{E}_o^* \end{Bmatrix} \delta n_e' = 0, \tag{C-2}$$

where

$$\underset{\approx}{\chi}(\Omega) = \begin{bmatrix} \Omega^2(\Omega^2-\omega_{ce}^2)^{-1} & -i\Omega\omega_{ce}(\Omega^2-\omega_{ce}^2)^{-1} & 0 \\ i\Omega\omega_{ce}(\Omega^2-\omega_{ce}^2)^{-1} & \Omega^2(\Omega^2-\omega_{ce}^2)^{-1} & 0 \\ 0 & 0 & 1 \end{bmatrix},$$

From (C-1) and (C-2) we obtain

$$(\mathbf{k}\pm\vec{\kappa})^2\epsilon_\pm\phi^\pm = i\,\frac{\omega_p^2}{\Omega^2}\,(\mathbf{k}+\vec{\kappa})\begin{Bmatrix}\underset{\approx}{\chi}(\Omega)\cdot\mathbf{E}_0 \\ \underset{\approx}{\chi}^*(\Omega)\cdot\mathbf{E}_0^*\end{Bmatrix}\delta n_e' .$$

b. *Ponderomotive potential.* The ponderomotive force [at $(\omega,\mathbf{k})$] on an electron in a magnetic field in the presence of high frequency electric fields $\mathbf{E}_0$, and $[-i(\mathbf{k}\pm\kappa)\phi^\pm]$ is $i\mathbf{k}\,\phi_p\,e$ where

$$\phi_p = \frac{e}{m_e\Omega^2}\,\{\mathbf{E}_0^*\cdot\underset{\approx}{\chi}\cdot[i(\mathbf{k}+\vec{\kappa})\phi^+] + [i(\mathbf{k}-\vec{\kappa})\phi^-]\cdot\underset{\approx}{\chi}\cdot\mathbf{E}_0\}$$

Inserting (C-3) into this expression for ϕ_p we obtain

$$4\pi k^2 e\phi_p = -|\mathbf{k}\cdot\Delta|^2\,e^2\delta n_e'\,[\frac{(e_+)^2}{\epsilon_-} + \frac{(e_-)^2}{\epsilon_-}], \qquad \text{(C-4)}$$

where $e_\pm = |[(\mathbf{k}\pm\vec{\kappa})\cdot\Delta]\,(\vec{\kappa}\cdot\Delta)^{-1}|$, and $\Delta = -e\underset{\approx}{\chi}\cdot\mathbf{E}_o/(m_e\Omega^2)$, and we have made use of the hermitian property of $\underset{\approx}{\chi}$

c. *Low frequency perturbations.* The electron and ion dielectric constants at $(\omega,\mathbf{k})$ (denoted ϵ_e and ϵ_i) give the density response to forces applied on the electronic and ionic plasma components, thus,

$$k^2\epsilon_e\,(\phi'+\phi_p) = 4\pi e\delta n_e', \qquad \text{(C-5a)}$$

$$k^2\epsilon_i\,\phi' = -4\pi e\delta n_i'. \qquad \text{(C-5b)}$$

(ϕ_p acts only on the electrons since $(m_e/m_i)\ll 1$.) In addition we have Poisson's equation for

the low frequency components

$$k^2\phi^l = 4\pi e(\delta n_e^l - \delta n_i^l) \ . \tag{C-6}$$

Eliminating ϕ_p, ϕ^l, δn_e^l and δn_i^l from (C-4)-(C-6) we obtain a general parametric desperison relation for electrostatic waves in an applied magnetic field

$$\epsilon + |\mathbf{k}\cdot\Delta|^2 \epsilon_e(1+\epsilon_i)[(e_+^2/\epsilon_+)+(e_-^2/\epsilon_-)] = 0, \tag{C-7}$$

where

$$\epsilon = 1+\epsilon_e(\omega, \mathbf{k}) + \epsilon_i \ (\omega, \mathbf{k}) \ .$$

In the dipole approximation ($\kappa << k$), we have $e_\pm \cong 1$.

Appendix D

VALIDITY OF THE ERGODIC INSTABILITY CONDITION, $<\gamma> > 0$

The exponentiation of wave energy is given by $\exp[2\int_0^t \gamma(t')\,dt']$, where the t' dependence of γ is due to the time dependence of $\mathbf{r}$ and $\mathbf{k}$, which evolve according to the ray equations. Defining $\gamma = <\gamma> + \Delta\gamma$ we can write

$$<\exp[2\int_0^t \gamma(t')\,dt']> \cong \exp[2<\gamma>t + 2<[\int_0^t \Delta\gamma(t')\,dt']^2>], \qquad \text{(D-1)}$$

which would be exactly true if $\int_0^t \Delta\gamma(t')\,dt'$ were a Gaussian random variable (which it is not). In order for $<\gamma> > 0$ to be a reasonable instability criterion, the second term in the exponent of (D-1) should be small compared to the first term, or

$$<\gamma>t >> <[\int_0^t \Delta\gamma(t')\,dt']^2> . \qquad \text{(D-2)}$$

Defining a correlation function $C(s) = <\Delta\gamma(t+s)\Delta\gamma(t)>$, and a correlation time τ_c, such that

$$<(\Delta\gamma)^2>\,\tau_c = 2\int_0^\infty C(s)\,ds ,$$

we can write (D-2) as

$$<\gamma> >> <(\Delta\gamma)^2>\,\tau_c , \qquad \text{(D-3)}$$

for $t >> \tau_c$. For the strongly ergodic case, τ_c is of the order of a radial transite time of the ray. Also, assuming $<(\Delta\gamma)^2> \sim (<\gamma>)^2$, (D-3) becomes

$$1 >> <\gamma>\,\tau_c .$$

Thus the average growth on one radial transit must be small in order for $<\gamma> > 0$ to be a

sensible instability condition. (This condition is required in any event, since, otherwise, even if $\langle\gamma\rangle < 0$, a *particular* ray path might lead to *e*-folding to large amplitude on one transit.)

REFERENCES

* Also at University of Maryland, College Park, MD. 20742

1. Three review articles with extensive lists of references are: V.A. Flyagin, A.V. Gaponov, M.I. Petelin and V.K. Yulpatov, IEEE Trans. **MTT-25**, 514 (1977); J.L. Hirshfield and V.L. Granatstein, **ibid.**, p. 522; P. Sprangle and A. Drobot **ibid.**, P. 528.

2. M. Read, R. Lucey, V.L. Granetstein, B. Hui, and K.R. Chu, Bull. Am. Phys. Soc. **43**, 749 (1978); V.V. Alikaev, G.A. Bobroviskii, V.I. Poznyak, K.A.Razumova, V.V. Sannikov, Yu. A. Sokolov, and A.A. Shmarin, Fiz. Plazmy **2**, 390 (1976) [Sov. J. Plasma Phys. **2**, 212 (1976)]

3. Recent theoretical works include the following: V. Alikaev, Yu. N. Dnestrovskii, V.V. Parail and G.V. Pereverzev, Fiz. Plazmy **3**, 230 (1977) [Sov. J. Plasma Phys. **3**, 127 (1977)]; A.G. Litvak, G.V. Permitin, E.V.Savorov, and A.A. Frajman, Nucl. Fusion **17**, 659 (1977); T.M. Antonsen and W.M. Manheimer, Phys. Fluids **21**, 2295 (1978); W.M. Manheimer in **Infrared and Millimeter Waves, Vol. 2**. Edited by K. Button (Academic Press, New York) to be published; I. Fidone, G. Granata, G. Ramponi, and R.L. Meyer, Phys. Fluids **21**, 645 (1978); O. Eldridge, W. Namkung, and A.C. England (to be published); T. Maekawa, S. Tanaka, Y. Terumichi, and Y. Hamada, Phys. Rev. Lett. **40**, 1379 (1978); S. M. Wolfe, D. R. Cohn, R. J. Temkin and K. Kreischer, Nucl. Fusion **19**, 389 (1979).

4. K.G. Budden, **Radio Waves in the Ionosphere** (Cambridge Universtiy Press, Cambridge, 1961), p. 123.

5. T.H. Stix, **The Theory of Plasma Waves** (McGraw-Hill, New York, 1962), pp. 55-59.

6. J.-M. Wersinger, E. Ott and J.M. Finn, Phys. Fluids **21**, 2263 (1978).

7. E. Ott, J.M. Wersinger, and P. Bonoli, Phys. Fluids **22**, 192 (1979).

8. V.D. Shafranov, in **Reviews of Plasma Physics, Vol. 2**, edited by M.A. Leontovich (Consultants Bureau, New York, 1966) pp. 125-131.

9. R.W. Conn and G.L. Kulcinski, Electric Power Research Institute Report ER-368(1976), Ch. 2.

10. T.H. Stix, Phys. Rev. Lett **15**, 878 (1965).

11. E. Ott, Phys. Fluids (to be published).

12. R.E. Slusher and C.M. Surko, Phys. Rev. Lett. **40**, 400 (1978).

13. E. Mazzucatto, Phys. Fluids **21**, 1063 (1978).

14. M. Porkolab, Nucl. Fusion **12**, 329 (1972). This paper considers homogeneous medium parametric instability for plasma heating near ω_{cc}.

15. H. Jory, private communication.

16. M.N. Rosenbluth, Phys. Rev. Lett. **29**, 565 (1972).

17. C.S. Liu, M.N. Rosenbluth, and R.B. White, Phys. Fluids **17**, 1211 (1974). Sec. V (D) deals with side scattering.

18. D.C. Montgomery and D.A. Tidman, **Plasma Kinetic Theory**, (McGraw-Hill, New York, 1964) Ch. 10.

19. W.M. Manheimer and E. Ott, Phys. Fluids **17**, 1413 (1974); J.F. Drake; P.K. Kaw, Y.C. Lee, G. Schmidt, C.S. Liu and M.N. Rosenbluth, Phys. Fluids **17**, 778 (1974); S. Johnston, A.N. Kaufman and G.L. Johnston, J. Plasma Phys. (to be published); E. Ott and C.T. Dum, Phys. Fluids **14**, 959 (1971).

20. M.A. Miller, Radiofizika **1**, (1958) [Sov. Radiophys. **1**, 110 (1958)]; J.R. Cary and A.N. Kaufman, Phys. Rev. Lett. **39**, 402 (1977); H. Motz and C. Watson, in Advances in Electronics and Electron Physics **23**, 153 (1967).

21. B. Hui, E. Ott K.R. Chu, and T. Antonsen (to be published).

Table I. Absorption characteristics of Type A Tokamaks ("small size")

MODE	ABSORPTION (%)	r_{max}/a	Θ	θ_o	ξ	$\frac{\omega_{po}}{\omega_{ce}^o}$	$T_e(0)$ (eV)	B_o (KG)	$N(0)$ (10^{13} cm^{-3})
O	11	0.03	5°	0°	0.8°	0.8	350	12	0.9
O	11	0.03	5°	10°	0.8°	0.8	350	12	0.9
O	10	0.03	5°	0°	0.8°	0.9	350	12	1.1
O	10	0.03	10°	0°	0.8°	0.8	350	12	0.9
X	19	0.03	30°	180°	0.8°	1.2	350	12	2.0
X	28	0.02	30°	180°	0.8°	1	350	12	1.4
X	39	0.02	30°	180°	0.8°	0.8	350	12	0.9
X	19	0.16	30°	135°	0.8°	1.2	350	12	2.0
X	46	0.02	40°	180°	0.8°	1	350	12	1.4

Table II. Absorption characteristics of Type B Tokamaks
("present-day size")

MODE	Relativistic	ABSORPTION (%)	$\frac{r_{max}}{a}$	Θ	θ_o	ξ	$\frac{\omega_{po}}{\omega_{ce}^o}$	$T_e(0)$ (KeV)	B_o (KG)	$N(0)$ (10^{13} cm^{-3})	$\frac{\omega}{\omega_{ce}^o}$
O	NO	100	0.05	5°	0°	0.6°	0.81	2.9	32	6.6	1
O	YES	100	0.02	5°	0°	0.6°	0.81	2.9	32	6.6	1
X	NO	1	0.0	0°	180°	0.5°	0.81	1.2	32	6.6	1
X	YES	53	0.01	0°	180°	0.5°	0.81	1.2	32	6.6	1
X	NO	100	0.29	30°	125°	0.36°	0.81	2.9	32	6.6	1
X	YES	100	0.33	30°	125°	0.36°	0.81	2.9	32	6.6	1
X	YES	100	0.34	30°	125°	0.5°	0.81	2.9	32	6.6	1
X	YES	100	0.38	30°	125°	5°	0.81	2.9	32	6.6	1
X	YES	100	0.42	30°	125°	10°	0.81	2.9	32	6.6	1
X	YES	100	0.09	30°	125°	0.36°	0.81	2.9	32	6.6	0.9

Table III. Absorption characteristics of Type C Tokamaks ("reactor size")

MODE	Relati-vistic	ABSORPTION (%)	$\frac{r_{max}}{a}$	Θ	θ_o	ξ	$\frac{\omega_{po}}{\omega_{ce}^o}$	$T_e(0)$ (KeV)	B_o (KG)	$N(0)$ $10^{14}(cm^{-3})$	$\frac{\omega}{\omega_{ce}^o}$
O	NO	100	0.04	5°	0°	0°	0.9	2.46	40.5	1.3	1
O	YES	100	0.01	5°	0°	0°	0.9	2.46	40.5	1.3	1
X	NO	100	0.13	10°	135°	0°	1.37	2.36	40.5	3	1
X	YES	100	0.21	10°	135°	0°	1.37	2.36	40.5	3	1
X	YES	100	0.13	10°	135°	0.5°	1.25	2.0	40.5	2.5	1.0
X	YES	100	0.26	10°	135°	5°	1.25	2.0	40.5	2.5	1.0
X	YES	100	0.37	10°	135°	10°	1.25	2.0	40.5	2.5	1.0
X	YES	100	0.02	10°	135°	0.5°	1.25	2.0	40.5	2.5	0.95
X	YES	100	0.28	10°	135°	0.5°	1.25	7.0	40.5	2.5	0.95

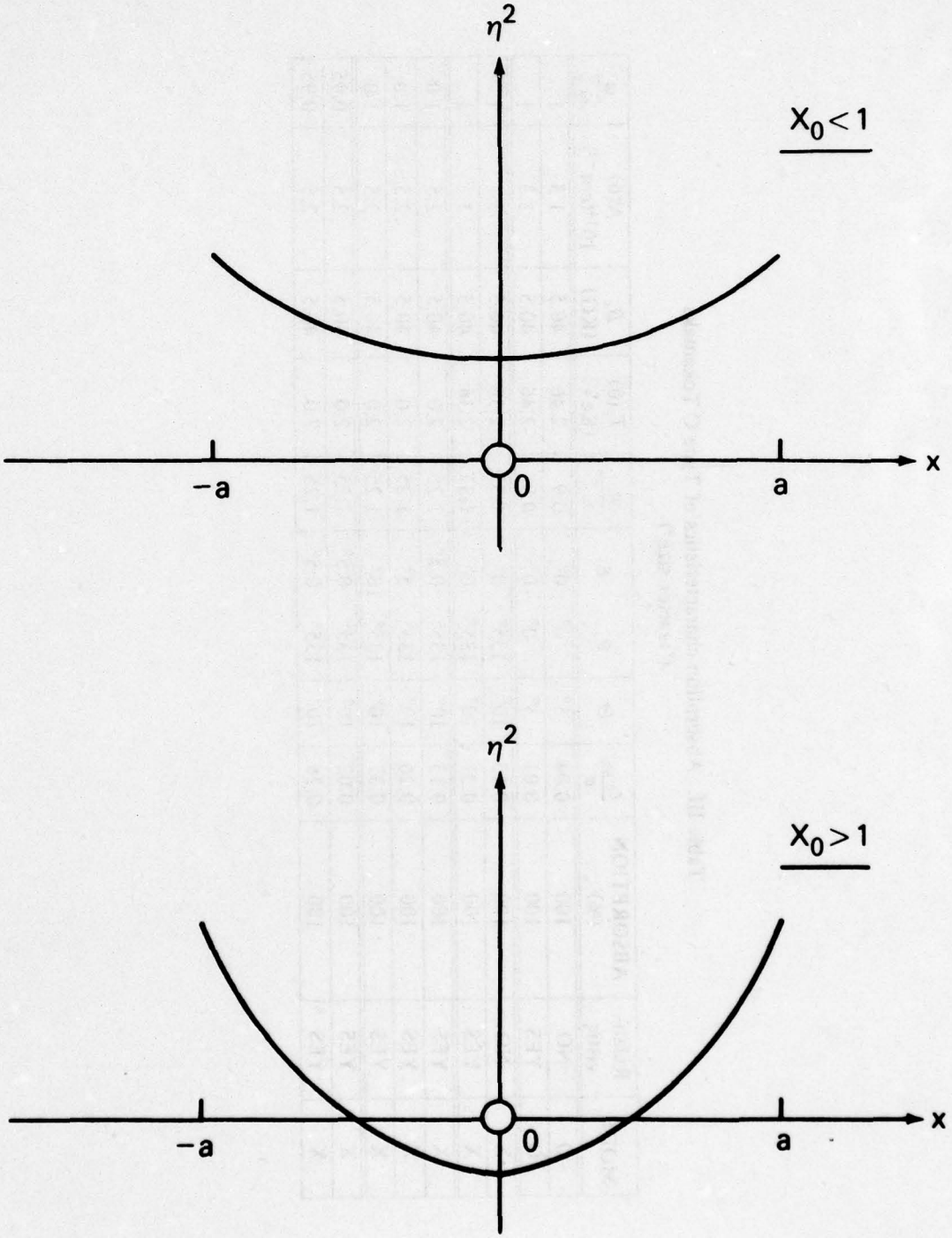

Fig. 1 — Refractive index versus x for the ordinary mode at normal incidence.

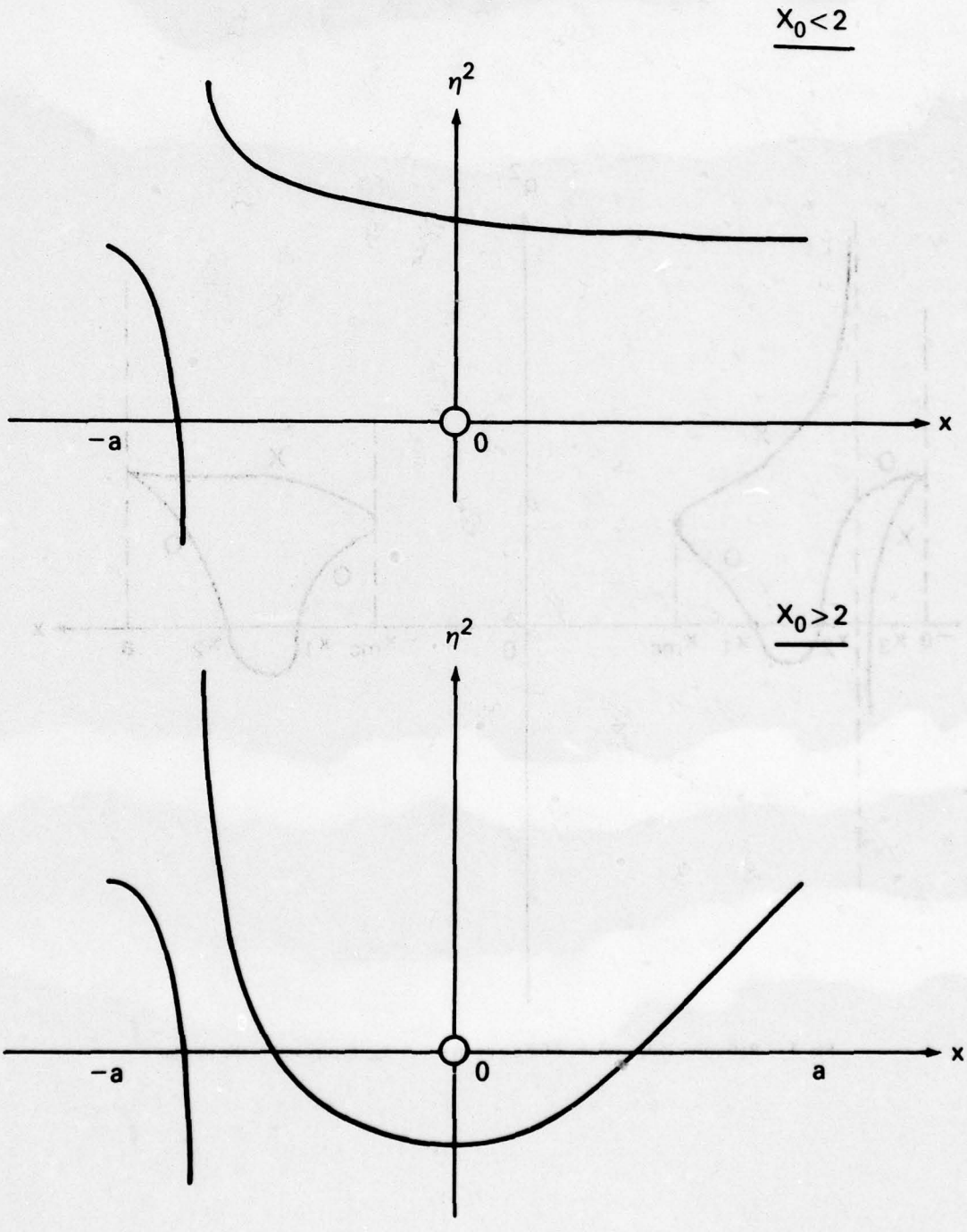

Fig. 2 — Refractive index versus x for the extradordinary wave mode at normal incidence.

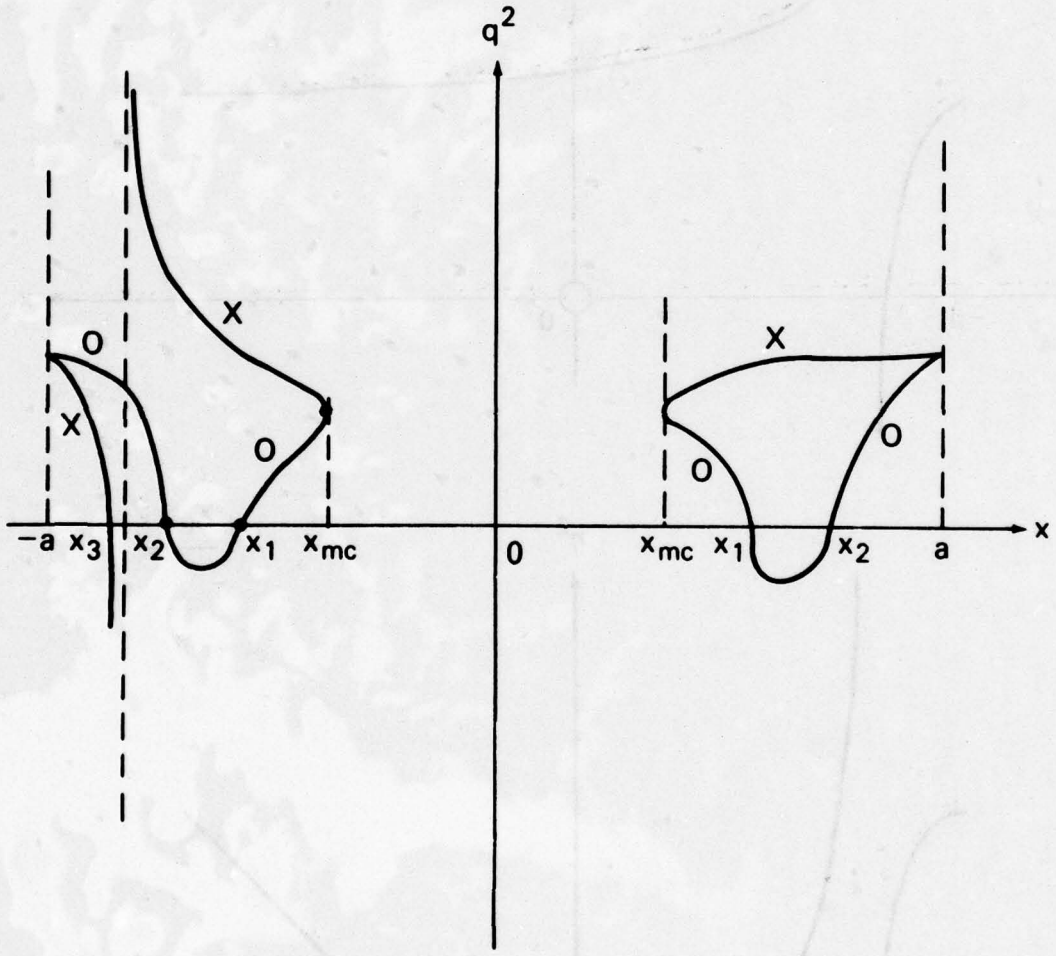

Fig. 3 — Refractive index versus x for a case in which X_{mc} occurs within the plasma.

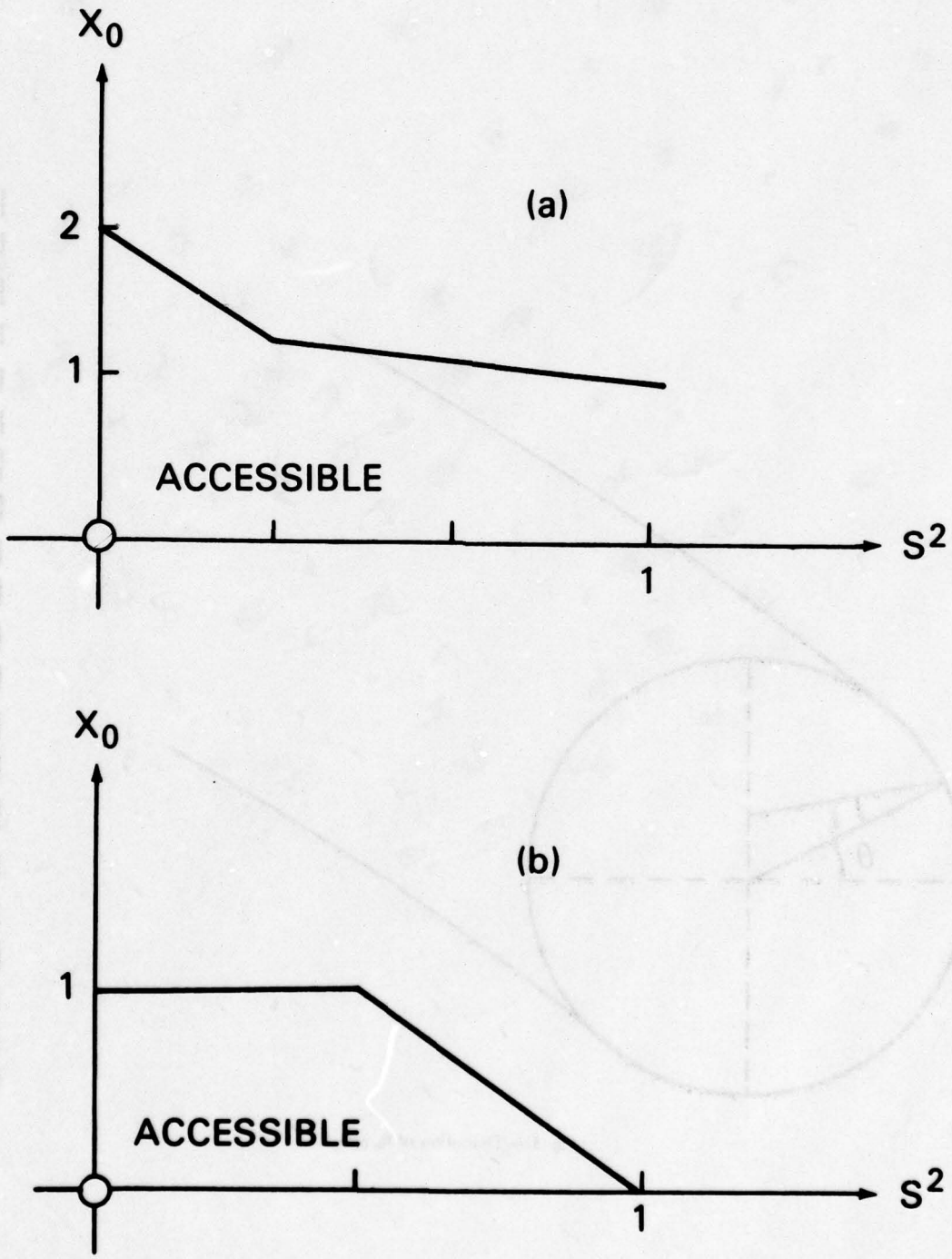

Fig. 4 — Maximum accessible value of ω_p^2/ω_{ce}^2 in the center of the plasma versus S^2 for (a) the extraordinary mode and (b) the ordinary mode.

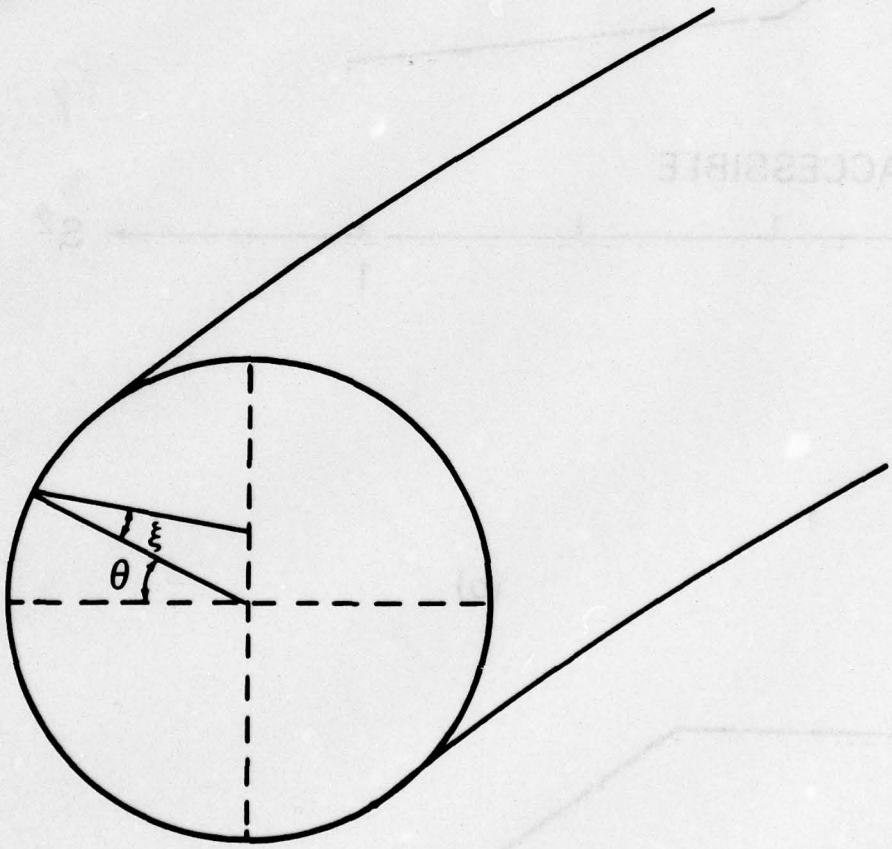

Fig. 5 — Definition of θ_0 and ξ.

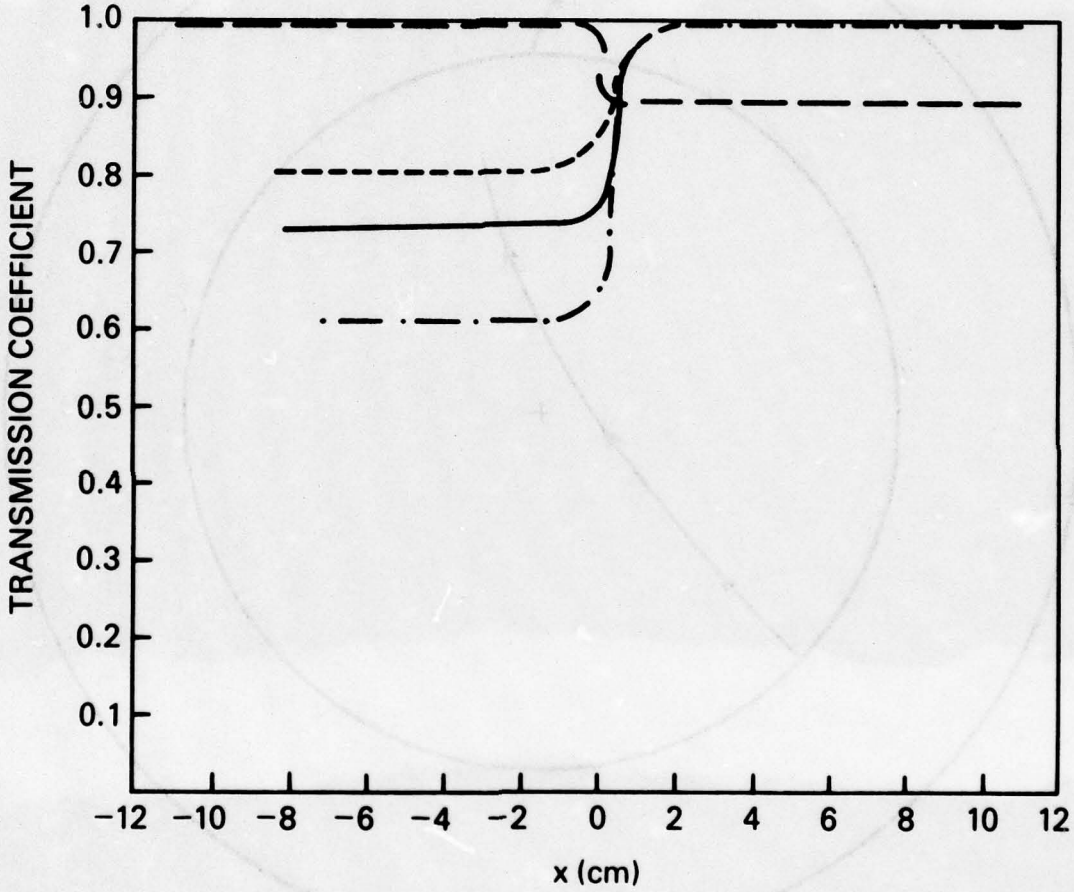

Fig. 6 — Transmission coefficient for the ordinary and extraordinary modes in a type A tokamak versus x. The long dash curve (— — —) is for the ordinary mode with $\omega_{p0}/\omega_{ce}^0 = 0.8$, $\Theta = 5°$, $\theta_0 = 0°$. The extraordinary mode is given by the short dash curve (---) for $\omega_{p0}/\omega_{ce}^0 = 1.2$, the solid curve (— — —) for $\omega_{p0}/\omega_{ce}^0 = 1.0$ and the dash dot curve (— · —) for $\omega_{p0}/\omega_{ce}^0 = 0.8$. For the three extraordinary mode cases $\Theta = 30°$, $\theta_0 = 180°$. In all cases $B_0 = 12$ KG and $T_e = 350$ eV.

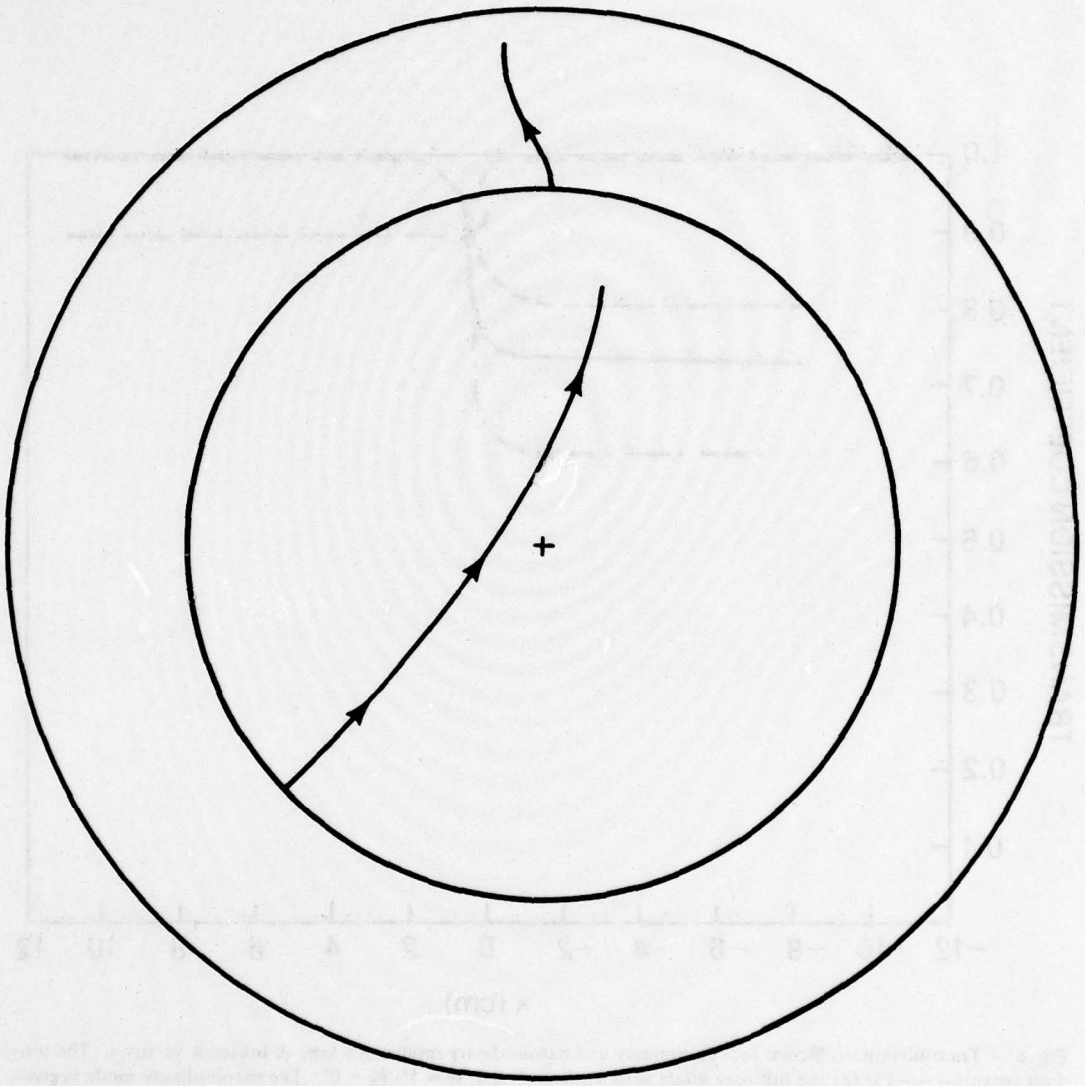

Fig. 7 — An example of a ray trajectory for a type A tokamak for the extradinary mode with $\Theta = 30°$, $\theta_0 = 135°$, $\omega_{p0}/\omega_{ce}^0 = 1.2$, $T_e(0) = 350$ eV and $B_0 = 12$ KG. The inner trace is in the poloidal plane and the outer trace is in the toroidal plane.

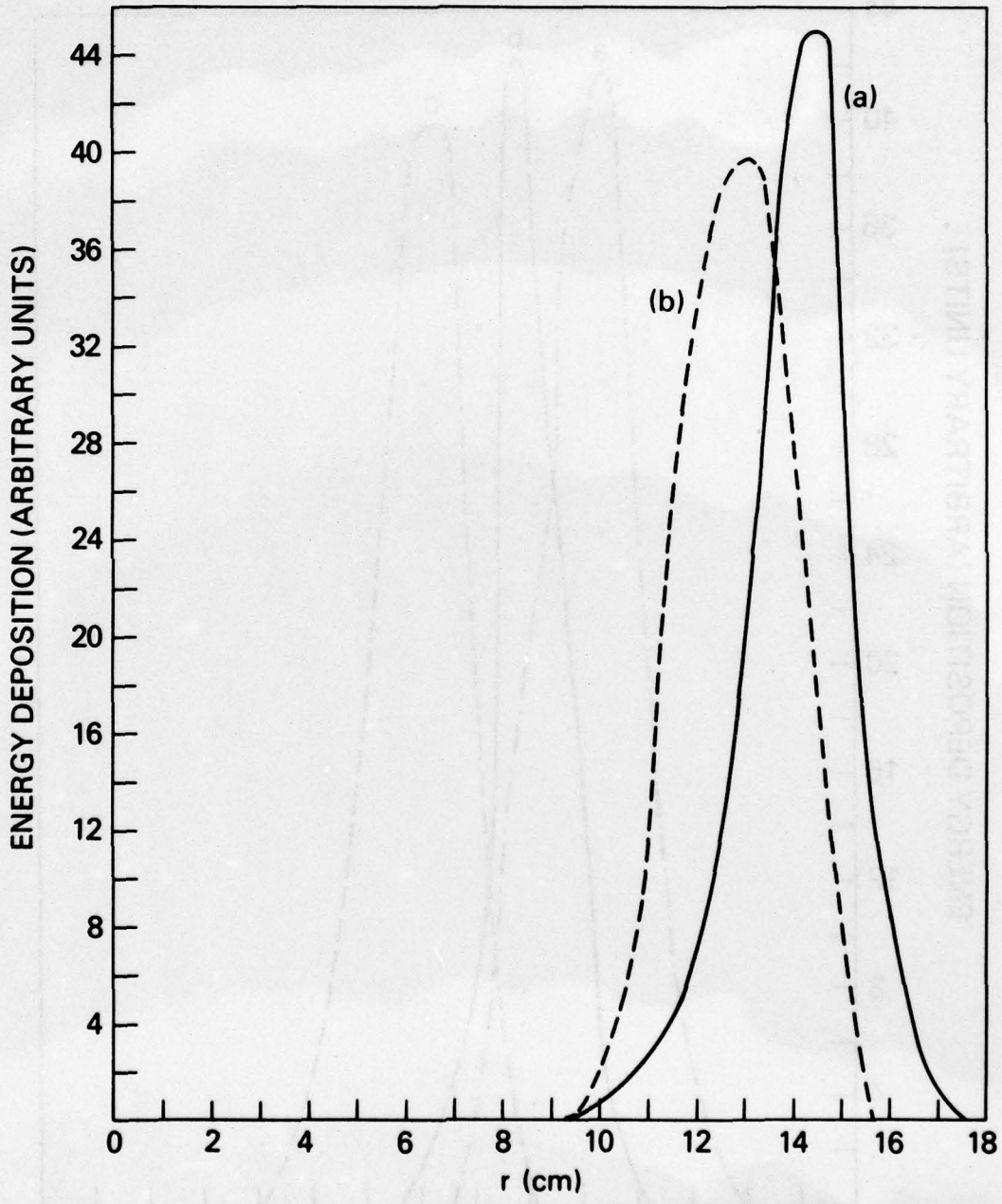

Fig. 8 — Energy deposition versus radius of magnetic surface r for a type B tokamak, (a) relativistic and (b) non relativistic. $\Theta = 30°$, $\theta_0 = 125°$, $\omega_{p0}/\omega_{ce}^0 = 0.81$, $T_e(0) = 2.9$ KeV and $B_0 = 32$ KG.

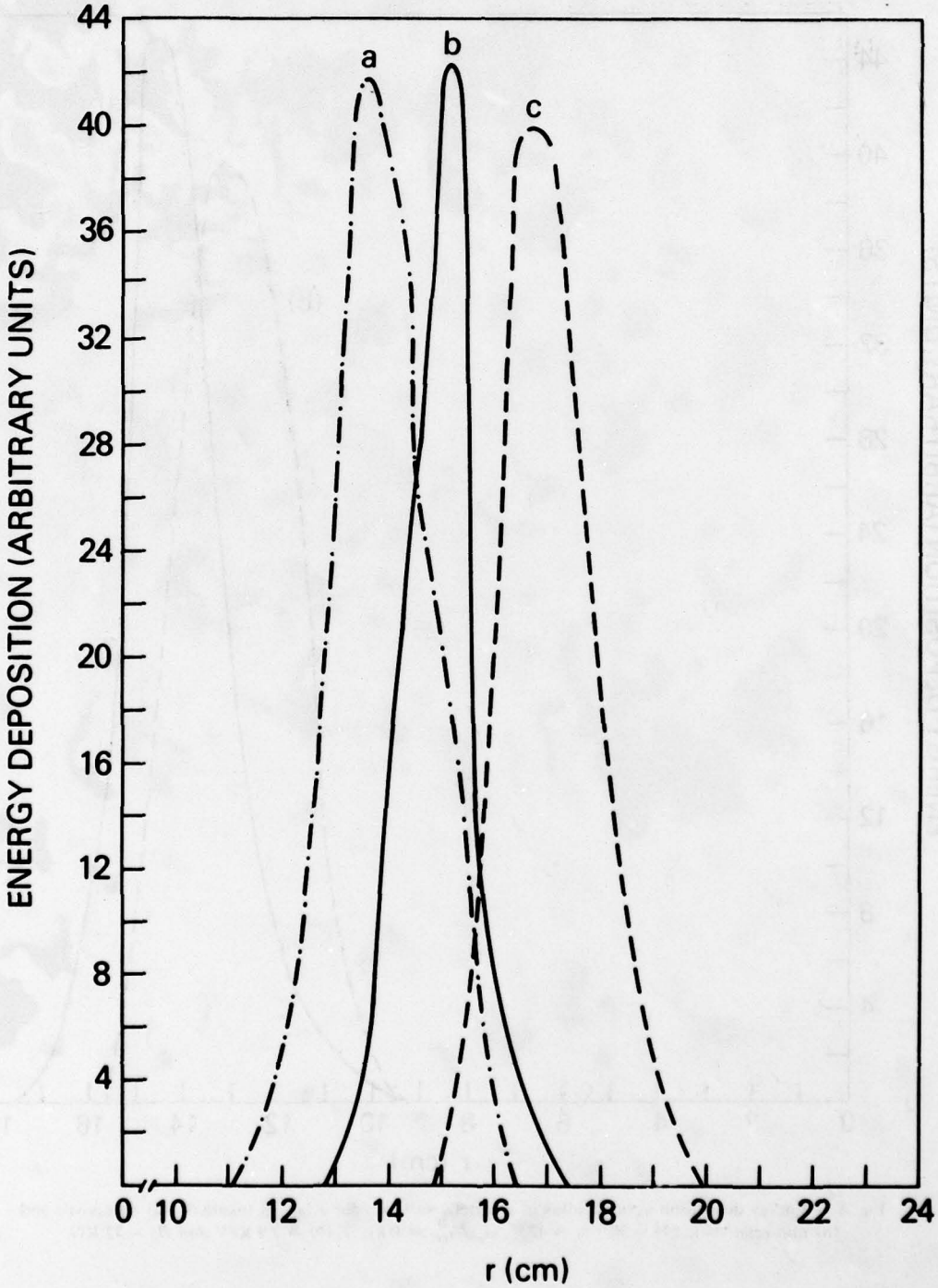

Fig. 9 — Energy deposition versus radius of magnetic surface r for a type B tokamak, (a) $\xi = 0.5°$ (b) $\xi = 5°$ and (c) $\xi = 10°$. $\Theta = 30°$, $\theta_0 = 125°$, $\omega_{p0}/\omega_{ce}^0 = 0.81$, $T_e(0) = 2.9$ KeV and $B_0 = 32$ KG.

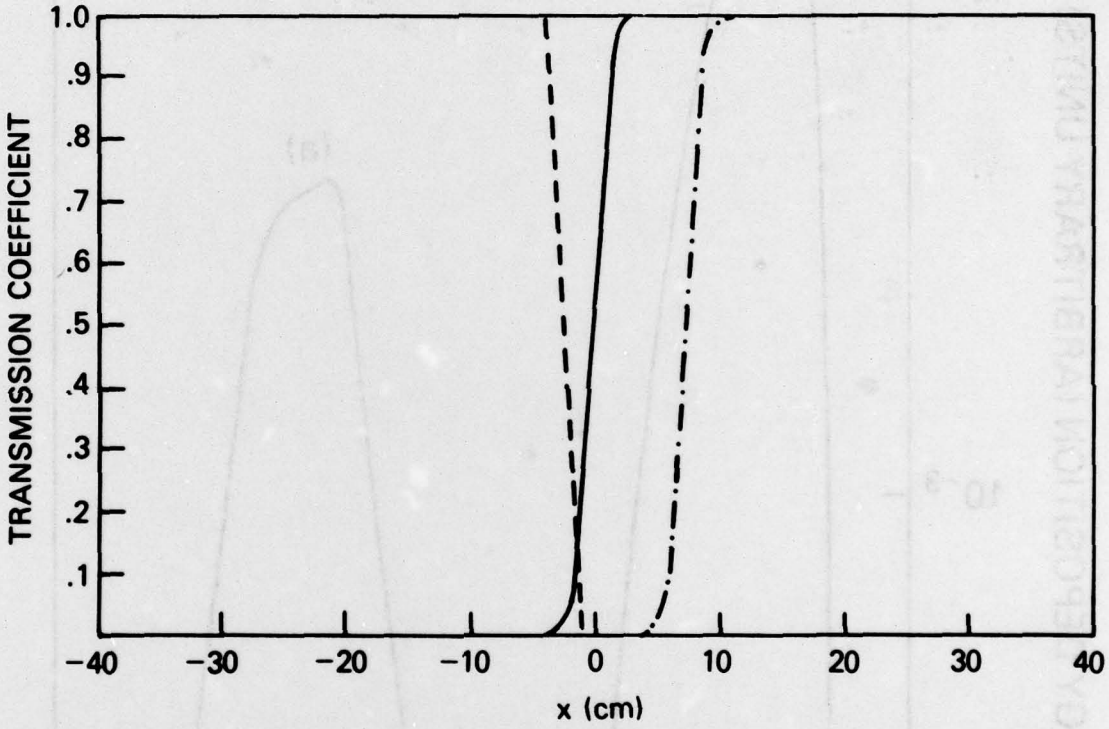

Fig. 10 — Transmission coefficient of ordinary and extraordinary modes in a type B tokamak versus $x = -r\cos\theta$. The dash curve (— — —) is for the ordinary mode with $\omega_{p0}/\omega_{ce}^{0} = 0.81$, $\Theta = 2°$ and $\theta_0 = 0°$. The extraordinary mode is the dash dot curve (— · —) with $\omega_{p0}/\omega_{ce}^{0} = 0.81$, $\Theta = 30°$, $\theta = 125°$; the solid curve has the same parameters but with $\omega = 0.9\ \omega_{ce}^{0}$. $B_0 = 32$ KG and $Te(0) = 2.89$ KeV.

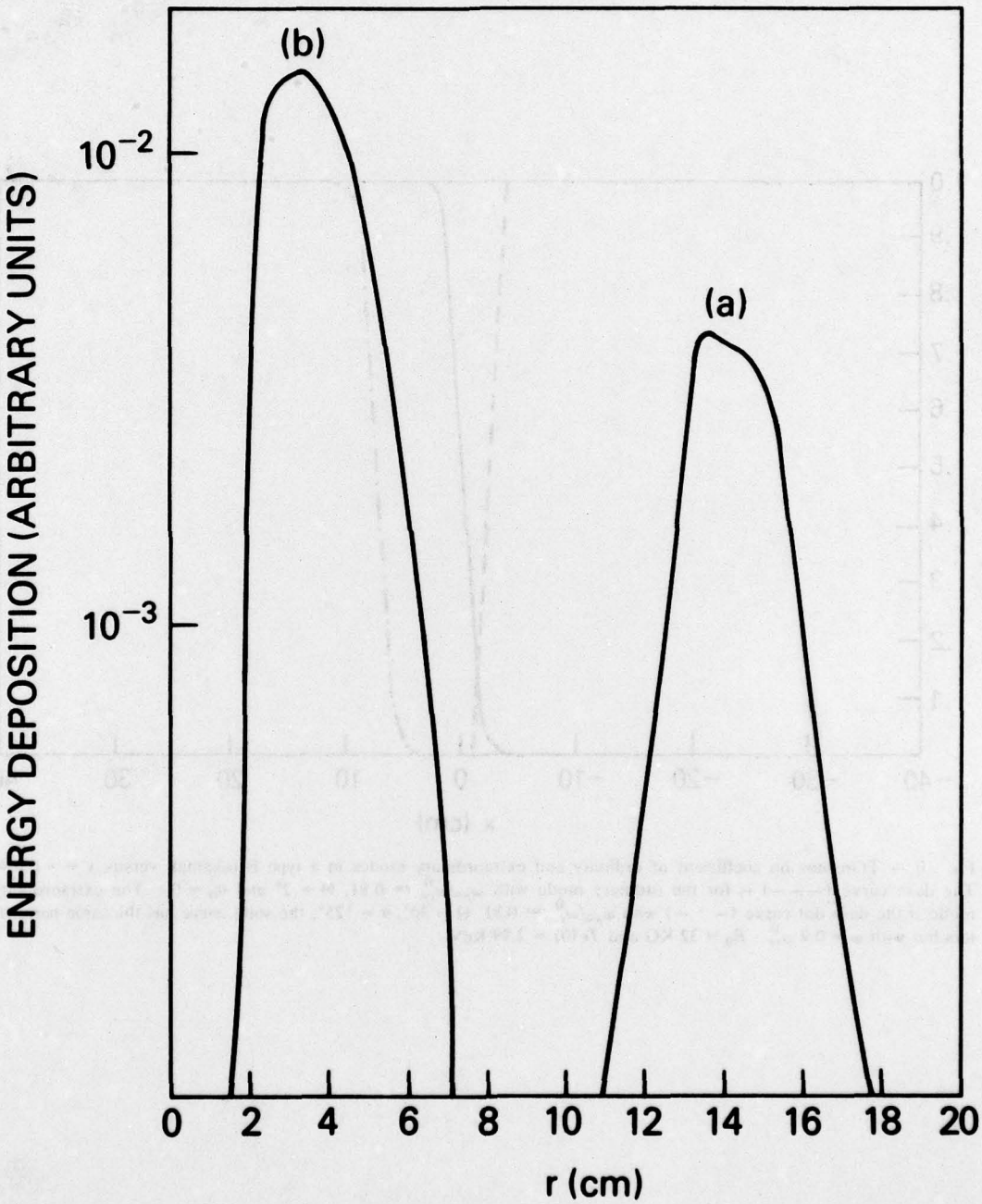

Fig. 11 — Energy deposition versus radius of magnetic surface r, (a) $\omega = \omega_{ce}^0$, (b) $\omega = 0.9\ \omega_{ce}^0$. $\omega_{p0}/\omega_{ce}^0 = 0.81$, $\Theta = 30°$, $\theta_0 = 125°$, $B = 32$ KG, $T_e(0) = 2.89$ KeV.

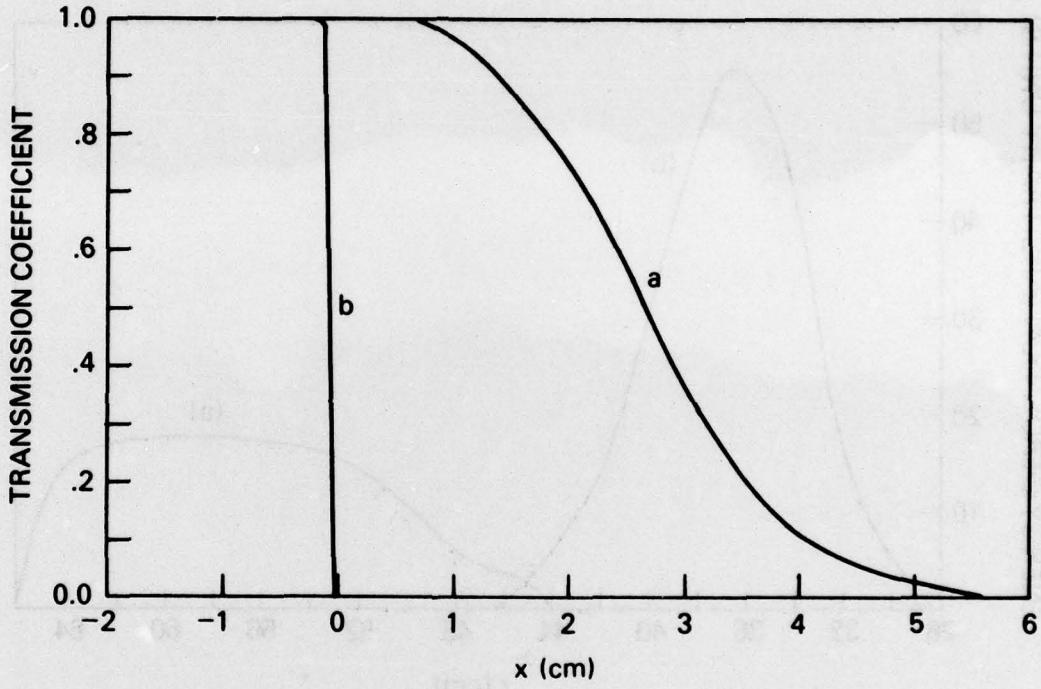

Fig. 12 — Transmission coefficient versus $x = -r\cos\theta$ for a type C tokamak, (a) relativistic, (b) non-relativistic. $\Theta = 5°$, $\theta_0 = 0°$, $\omega_{p0}/\omega_{ce}^{0} = 0.9$, $T_e(0) = 2.46$ KeV and $B_0 = 40.5$ KG.

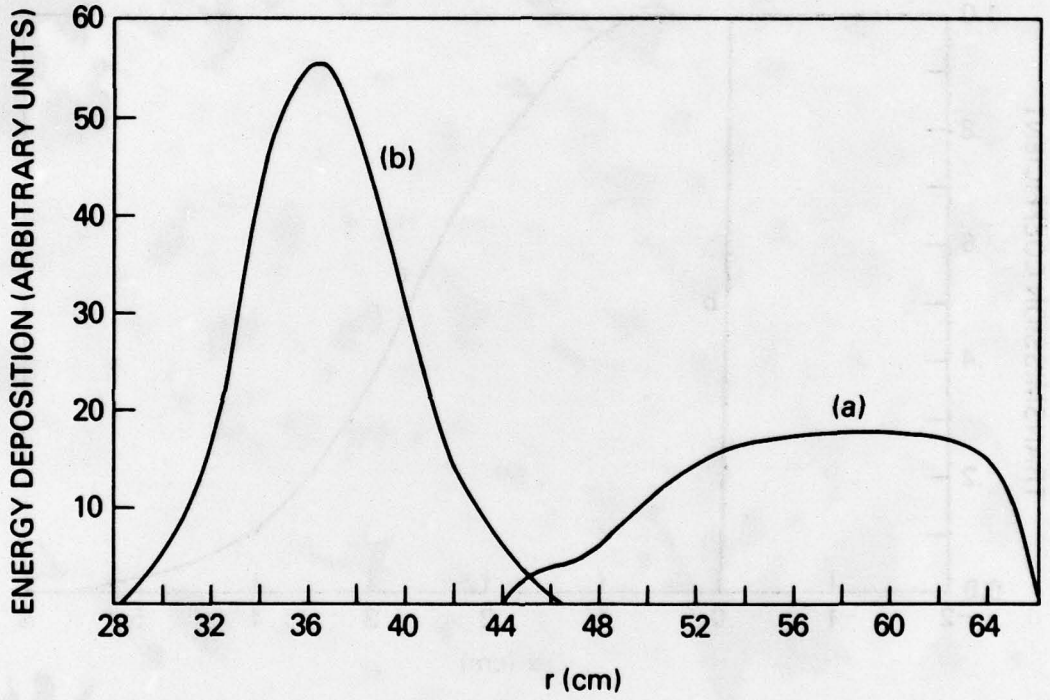

Fig. 13 — Energy deposition vs r for a type C tokamak, (a) relativistic, (b) nonrelativistic. $\Theta = 2°$, $\theta_0 = 0°$, $\omega_{p0}/\omega_{ce}^0 = 0.9$, $T_e(0) = 2.46$ KeV, and $B_0 = 40.5$ KG.

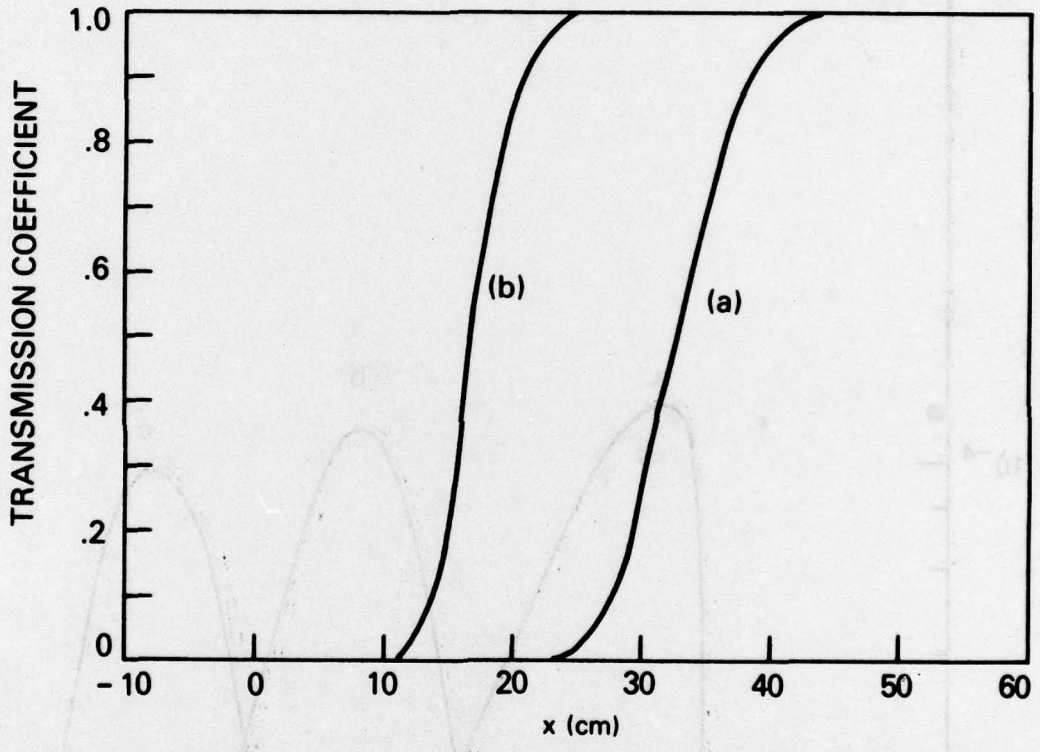

Fig. 14 — Transmission coefficient versus x for a type C tokamak (a) relativistic and (b) nonrelativistic. $\Theta = 10°$, $\theta_0 = 135°$, $\omega_{p0}/\omega_{ce}^0 = 1.37$, $T_e(0) = 2.38$ KeV and $B_0 = 40.5$ KG.

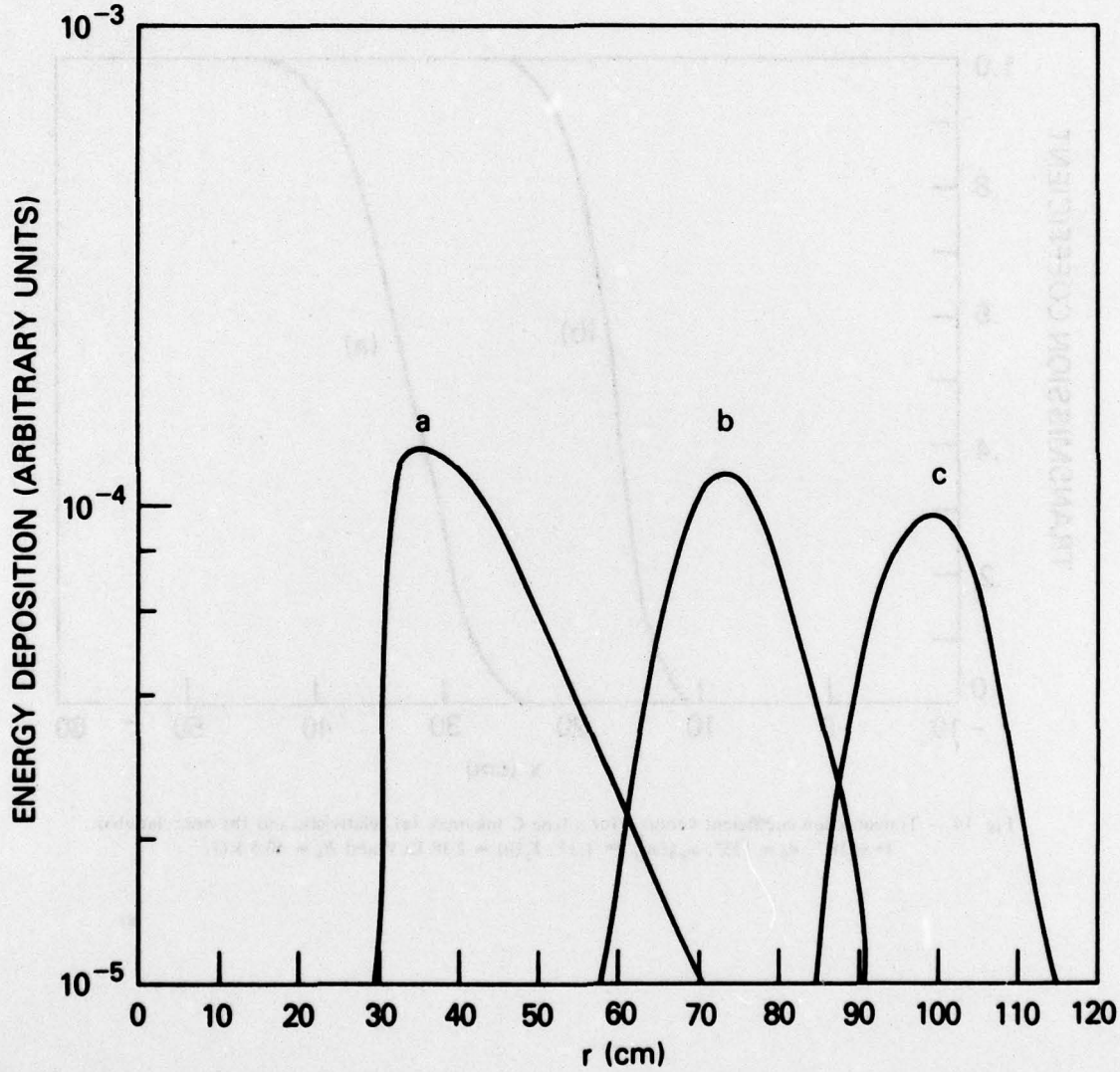

Fig. 15 — Energy deposition versus r for a type C tokamak, (a) $\xi = 0.5°$, (b) $\xi = 5°$ and (c) $\xi = 10°$. $\Theta = 10°$, $\theta_0 = 135°$, $T_e(0) = 2.0$ KeV, $B = 40.5$ KG, $\omega_{p0}/\omega_{ce}^0 = 1.25$ and $\omega/\omega_{ce}^0 = 1.0$

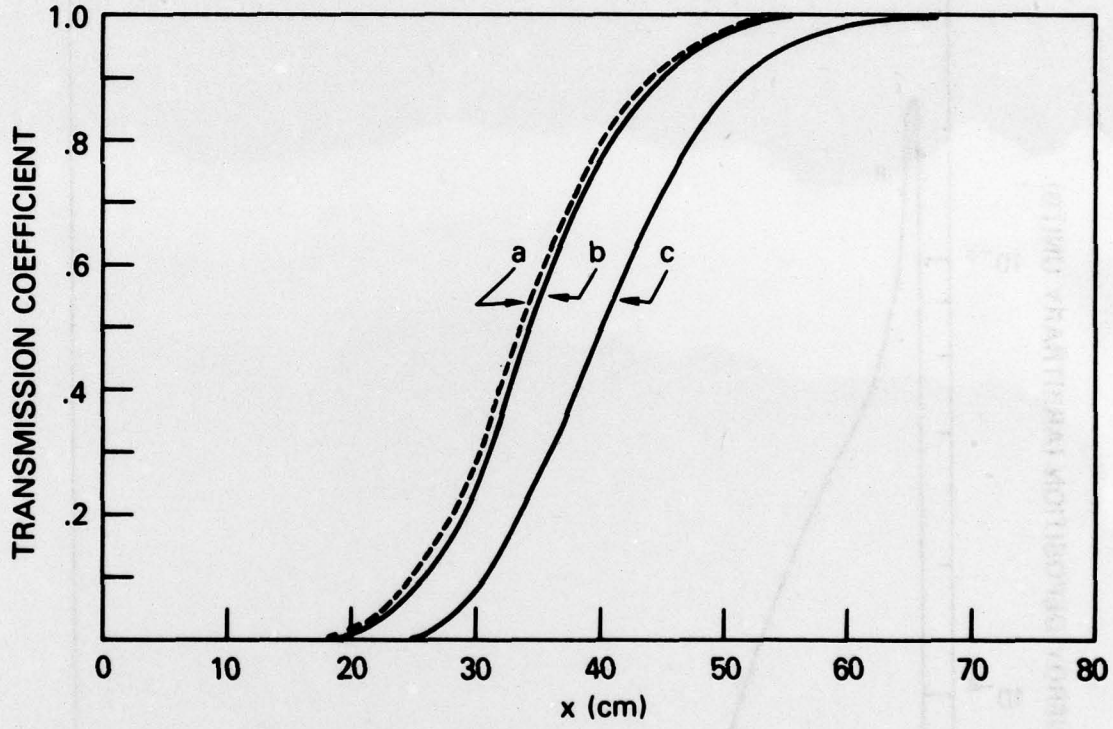

Fig. 16 — Transmission coefficient versus x for a type C tokamak. (a) $\xi = 0.5°$, (b) $\xi = 5°$ and (c) $\xi = 10°$. $\Theta = 10°$, $\theta_0 = 135°$, $T_e(0) = 2.0$ KeV, $B = 40.5$ KG, $\omega_{p0}/\omega_{ce}^0 = 1.25$ and $\omega/\omega_{ce}^0 = 1.0$.

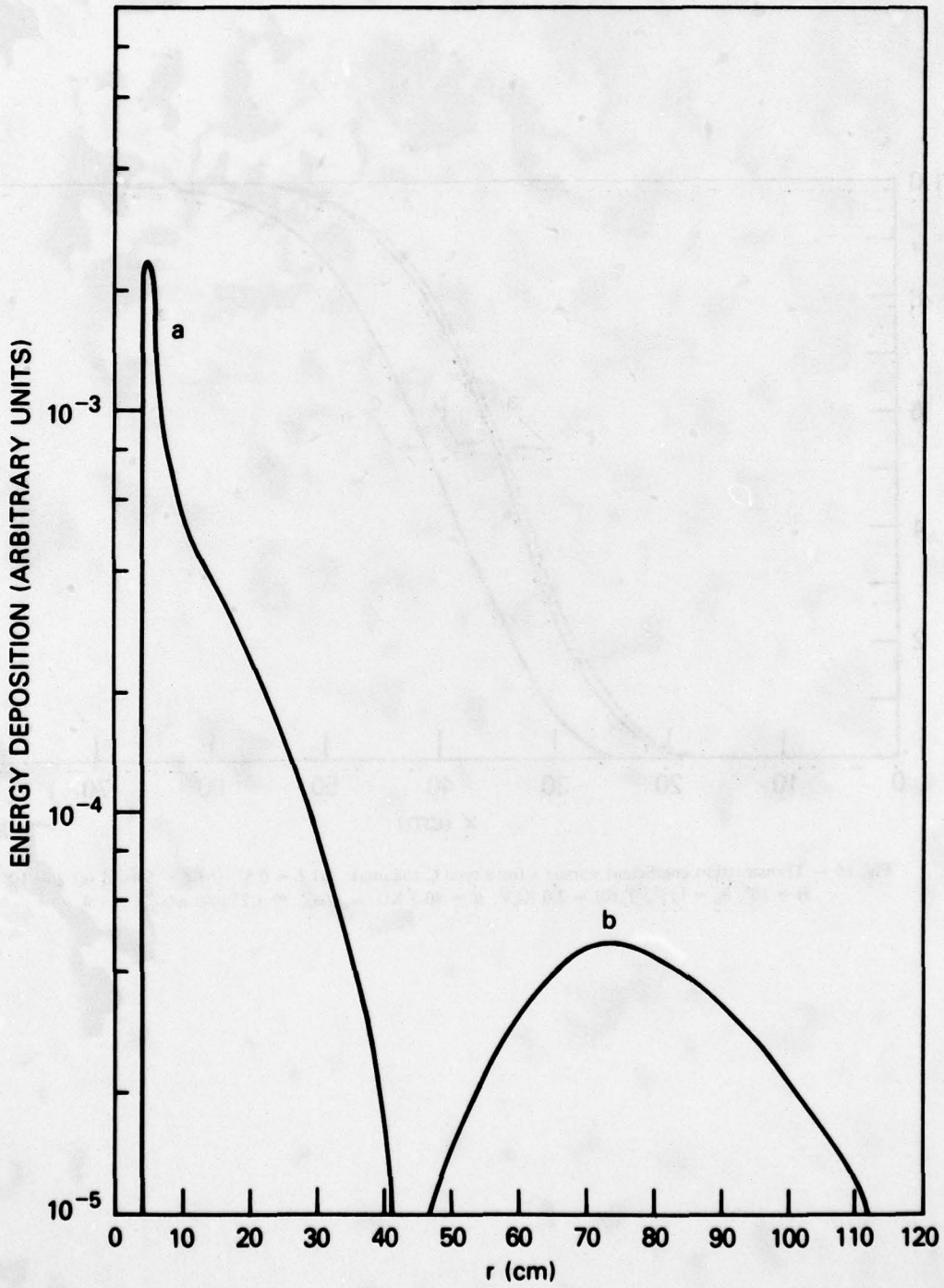

Fig. 17 — Energy deposition versus r for a type C tokamak, (a) $T_e(0) = 2$ KeV and (b) $T_e(0) = 7$ KeV. $\Theta = 10°$, $\theta_0 = 135°$, $B_0 = 40.5$ KG and $\omega/\omega_{ce}^0 = 0.95$.

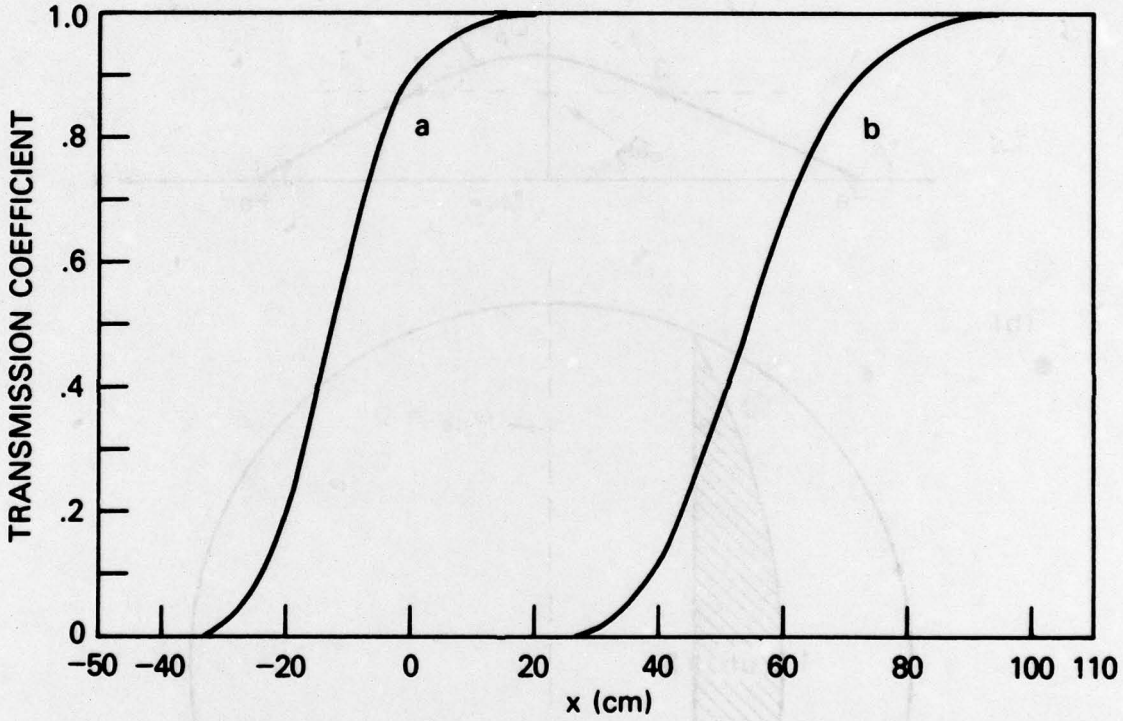

Fig. 18 — Transmission coefficient versus x for a type C tokamak, (a) $T_e(0) = 2$ KeV and (b) $T_e(0) = 7$ KeV. $\Theta = 10°$, $\theta_0 = 135°$, $\omega_{p0}/\omega_{ce}^0 = 1.25$, $B_0 = 40.5$ KG and $\omega/\omega_{ce}^0 = 0.95$.

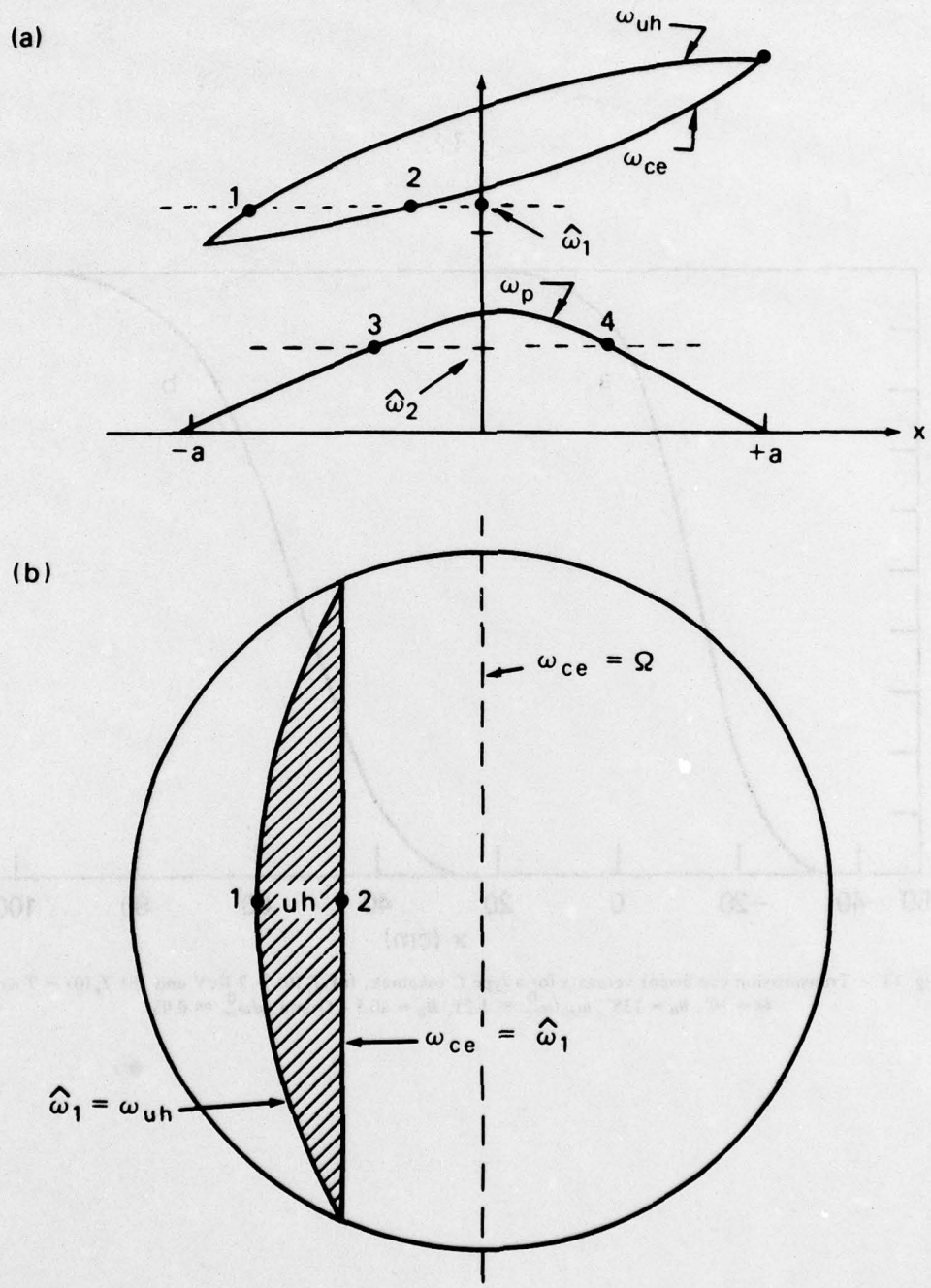

Fig. 19 — (a) Upper hybrid frequency (ω_{uh}), electron cyclotron frequency (ω_{ce}), and plasma frequency (ω_p) versus position, $x = R_0 - R$, where R is the major radius and R_0 is the major radius at the center of the minor cross-section ($r = 0$). $\hat{\omega}_1$ and $\hat{\omega}_2$ are frequencies of possible decay waves ($\hat{\omega}_1, \hat{\omega}_2 < \omega_{ce}^0$). The density of low, i.e. $\omega_p < \omega_{ce}$ everywhere. (b) Propagation region for a cold plasma decay wave with frequency ω_1 (an upper hybrid wave). (Ω is the pump frequency.) (c) Propagation region for a cold plasma decay wave with frequency $\hat{\omega}_2$ (a lower hybrid wave).

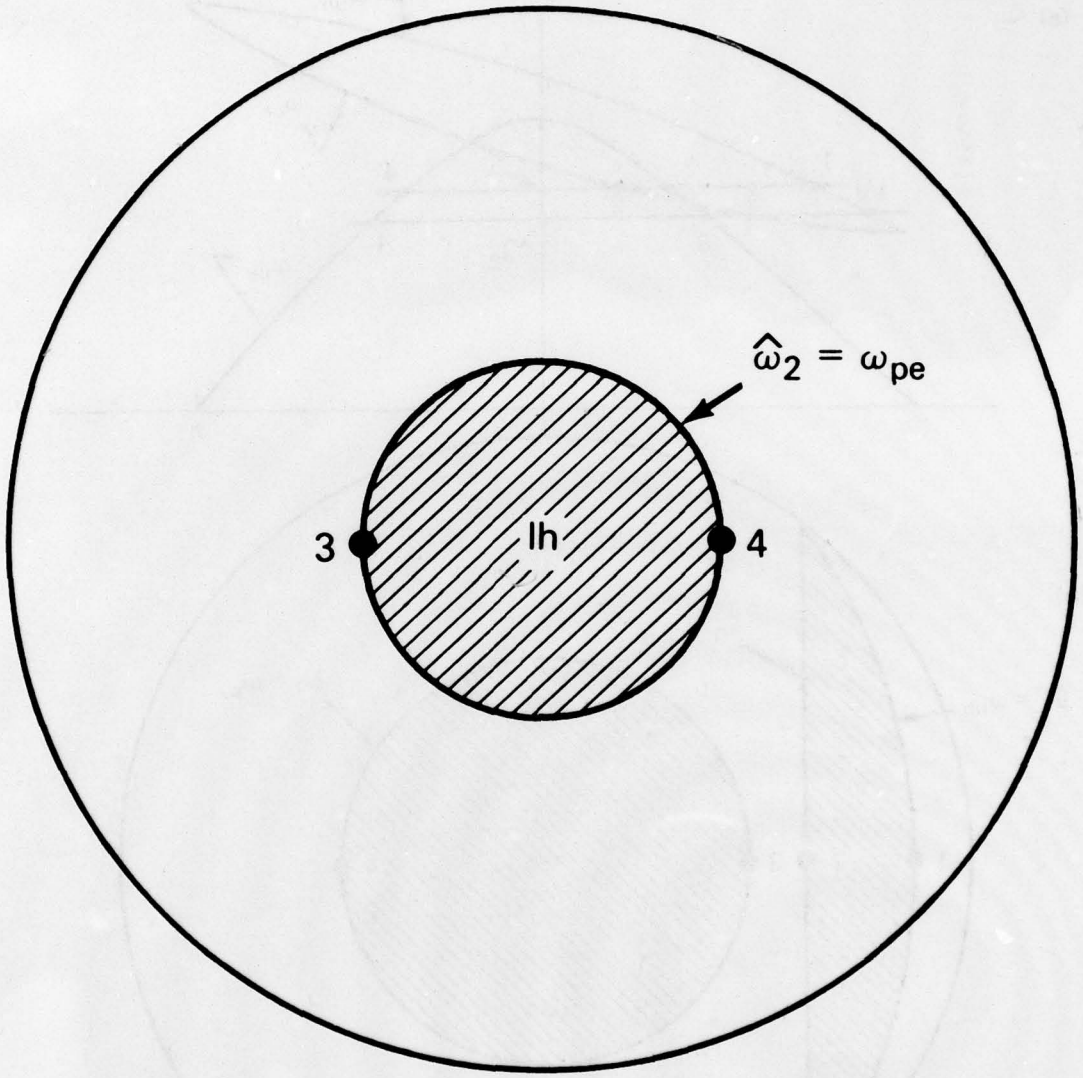

(c)

Fig. 19 (continued) — (a) Upper hybrid frequency (ω_{uh}), electron cyclotron frequency (ω_{ce}), and plasma frequency (ω_p) versus position, $x = R_0 - R$, where R is the major radius and R_0 is the major radius at the center of the minor cross-section ($r = 0$). $\hat{\omega}_1$ and $\hat{\omega}_2$ are frequencies of possible decay waves ($\hat{\omega}_1, \hat{\omega}_2 < \omega_{ce}^0$). The density of low, i.e. $\omega_p < \omega_{ce}$ everywhere. (b) Propagation region for a cold plasma decay wave with frequency ω_1 (an upper hybrid wave). (Ω is the pump frequency.) (c) Propagation region for a cold plasma decay wave with frequency $\hat{\omega}_2$ (a lower hybrid wave).

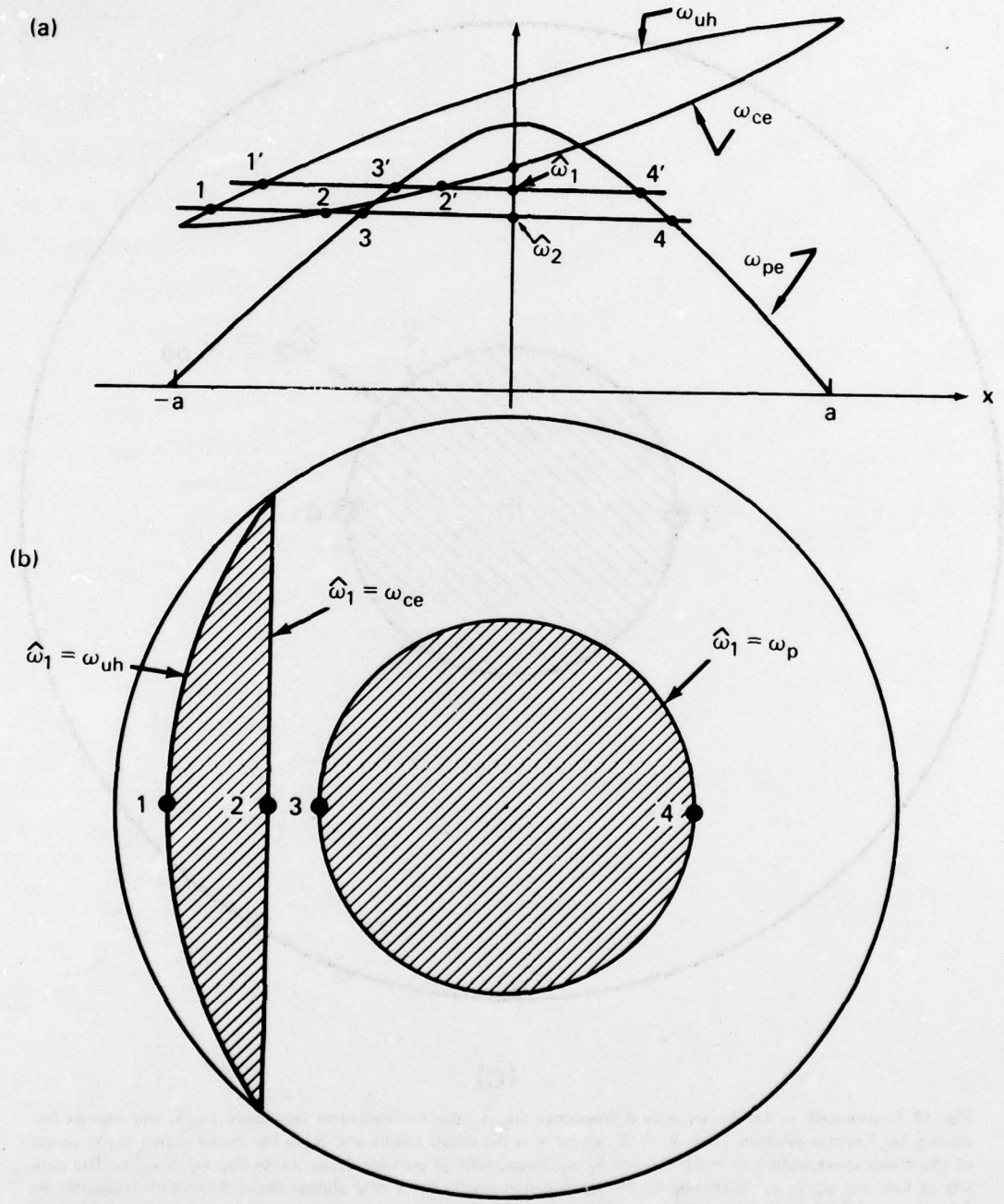

Fig. 20 — (a) Same as Fig. 19 (a), but with a higher density, $\omega_{p0} > \omega_{ce}^0$; (b) and (c) show regions of propagation for decay waves with frequencies $\hat{\omega}_1$ and $\hat{\omega}_2$.

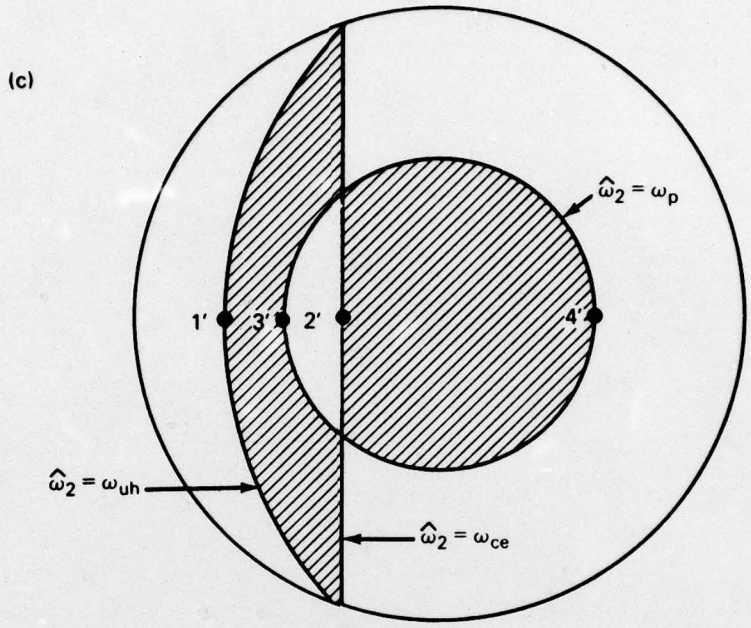

Fig. 20 (continued) — (a) Same as Fig. 19 (a), but with a higher density, $\omega_{pi} > \omega_{ce}^{o}$; (b) and (c) show regions of propagation for decay waves with frequencies $\hat{\omega}_1$ and $\hat{\omega}_2$.

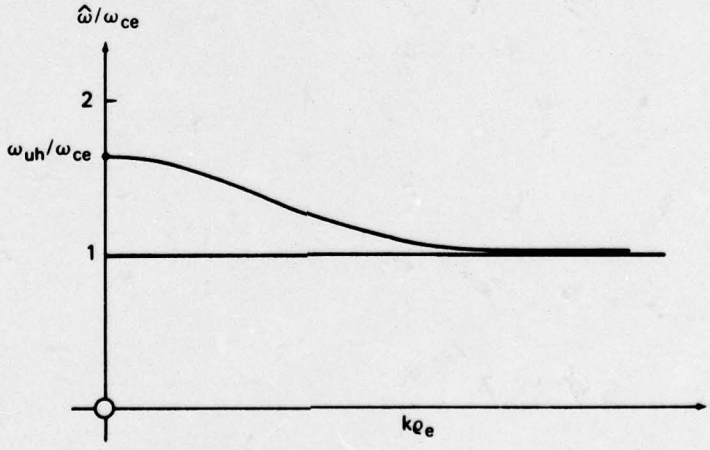

Fig. 21 — Bernstein mode dispersion for $\hat{k}_{\parallel} = 0$ and $\omega_{pi}^2/\omega_{ce}^2 < 3$.